ACS NANO

www.acsnano.org

ARTICLE

# Molecular-Targeted Immunotherapeutic Strategy for Melanoma *via* Dual-Targeting Nanoparticles Delivering Small Interfering RNA to Tumor-Associated Macrophages

Yuan Qian,[†,‡,§] Sha Qiao,[†,‡,§] Yanfeng Dai,[†,‡] Guoqiang Xu,[†,‡] Bolei Dai,[†,‡] Lisen Lu,[†,‡] Xiang Yu,[†,‡] Qingming Luo,[†,‡] and Zhihong Zhang*[,†,‡]

[†]Britton Chance Center for Biomedical Photonics, Wuhan National Laboratory for Optoelectronics—Huazhong University of Science and Technology, Wuhan, Hubei 430074, China

[‡]MoE Key Laboratory for Biomedical Photonics, Collaborative Innovation Center for Biomedical Engineering, School of Engineering Sciences, Huazhong University of Science and Technology, Wuhan, Hubei 430074, China

Supporting Information

**ABSTRACT:** **Tumor-associated macrophages (TAMs) are a promising therapeutic target for cancer immunotherapy. Targeted delivery of therapeutic drugs to the tumor-promoting M2-like TAMs is challenging. Here, we developed M2-like TAM dual-targeting nanoparticles (M2NPs), whose structure and function were controlled by α-peptide (a scavenger receptor B type 1 (SR-B1) targeting peptide) linked with M2pep (an M2 macrophage binding peptide). By loading anti-colony stimulating factor-1 receptor (anti-CSF-1R) small interfering RNA (siRNA) on the M2NPs, we developed a molecular-targeted immunotherapeutic approach to specifically block the survival signal of M2-like TAMs and deplete them from melanoma tumors. We confirmed the validity of SR-B1 for M2-like TAM targeting and demonstrated the synergistic effect of the two targeting units (α-peptide and M2pep) in the fusion peptide (α-M2pep). After being administered to tumor-bearing mice, M2NPs had higher affinity to M2-like TAMs than to tissue-resident macrophages in liver, spleen, and lung. Compared with control treatment groups, M2NP-based siRNA delivery resulted in a dramatic elimination of M2-like TAMs (52%), decreased tumor size (87%), and prolonged survival. Additionally, this molecular-targeted strategy inhibited immunosuppressive IL-10 and TGF-β production and increased immunostimulatory cytokines (IL-12 and IFN-γ) expression and CD8⁺ T cell infiltration (2.9-fold) in the tumor microenvironment. Moreover, the siRNA-carrying M2NPs down-regulated expression of the exhaustion markers (PD-1 and Tim-3) on the infiltrating CD8⁺ T cells and stimulated their IFN-γ secretion (6.2-fold), indicating the restoration of T cell immune function. Thus, the dual-targeting property of M2NPs combined with RNA interference provides a potential strategy of molecular-targeted cancer immunotherapy for clinical application.**

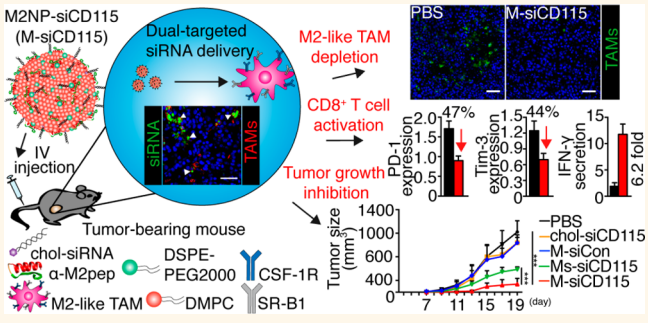


**KEYWORDS:** *tumor-associated macrophage, dual-targeting, cancer immunotherapy, colony stimulating factor-1 receptor, small interfering RNA*

Malignant tumors, such as melanoma, often end in recurrence because patients respond deficiently to the generally used therapies including radiation, chemotherapy, and surgery.[1,2] Rather than focusing on directly killing tumor cells, cancer immunotherapy aims to produce a long-lasting immunosurveillance effect to avoid relapse by restoring the antitumor immunity in the tumor microenvironment.[3,4] Tumor-associated macrophages (TAMs), one of the most abundant tumor-infiltrating leukocytes in various tumors, tend to polarize to an alternative activated M2 rather than the classical activated M1 phenotype.[5,6] Hence, TAMs generally exhibit numerous tumor-promoting properties derived from their M2 polarization phenotype, such as promotion of angiogenesis through expressing vascular endothelial growth factor (VEGF) and restraining the adaptive immune responses

Received: August 1, 2017
Accepted: August 31, 2017
Published: August 31, 2017




DOI: 10.1021/acsnano.7b05465
*ACS Nano* 2017, 11, 9536–9549

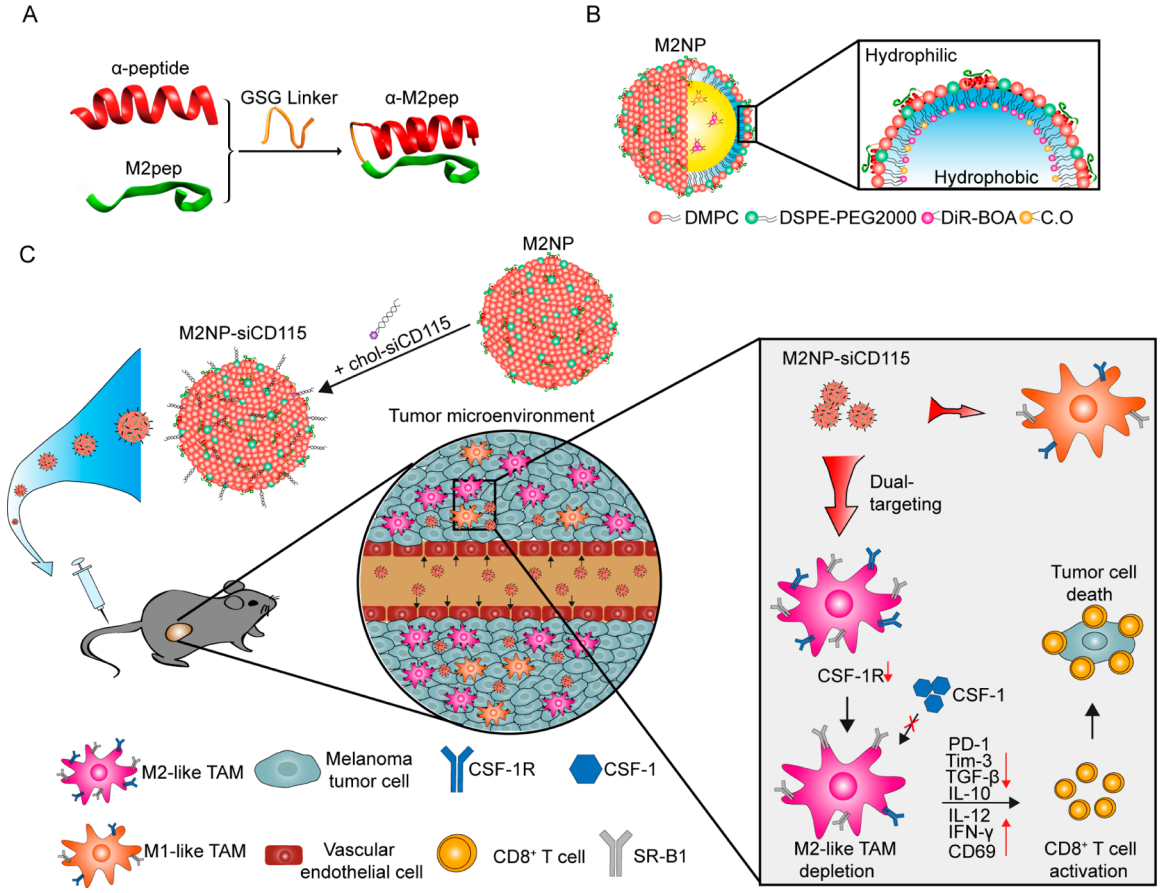


**Figure 1. Design of the M2NP for M2-like TAM-specific molecular-targeted immunotherapy. (A) Hybrid approach of the fusion peptide α-M2pep. (B) Structure and components of M2NP. (C) M2NP-based delivery of siRNA for CSF-1R silencing and immune regulation *via* synergistic dual targeting of M2-like TAMs *in vivo*.**

by inducing the dysfunction in dendritic cells (DCs) and $CD8^+$ T cells.[7,8] Therefore, TAMs represent an attractive target for cancer immunotherapy.

At present, in order to reverse the immunosuppressive tumor microenvironment initiated by M2-like TAMs, the most widely used therapeutic strategy is either depleting or re-educating them using nontargeted drugs, such as trabectedin and zoledronic acid.[9,10] However, there exists a safety issue about these nontargeted treatments because of the key role of macrophages in innate immunity and their whole-body distribution.[10,11] Therefore, there is an urgent need for a carrier with M2-like TAM-targeting ability. Functioning through phagocytic capacity of TAMs or ligands, such as mannose and folate, previously reported nanoplatforms showed TAM affinity and promising therapeutic results.[12−14] However, besides macrophages, DCs and B cells also represent major components of phagocytes. Moreover, while targeting to TAMs, mannose and folate bind to other cell populations, such as DCs, epithelial cells, and even tumor cells.[15−17] Therefore, developing more specific binding entities is a major focus of M2-like TAM-targeted therapy. Recently, Cieslewicz *et al.* had reported a peptide, designated as M2pep, that possesses higher specificity to M2-like TAMs than other leukocytes.[18] Nevertheless, the poor drug-loading capacity of peptides limits the direct application of M2pep. Hence, nanocarriers equipped with both M2-like TAM-specific targeting entities and therapeutic drugs are appealing.

The CSF-1/CSF-1R pathway is crucial for the differentiation and survival of macrophages. Overexpression of CSF-1 and CSF-1R (CD115) often correlates with poor prognosis.[19,20] Unlike CSF-1, which is expressed by various populations of cells in the tumor area, CSF-1R is restrictively expressed by TAMs and monocytes (precursors of macrophages).[21] Therefore, CSF-1R blocking is a particularly specific strategy against TAMs and their pro-tumor effects. Small molecular inhibitors (such as GW2580 and BLZ945) and antibodies against CSF-1R have been used for depleting or re-educating TAMs.[21,22] Compared with these therapeutic drugs, siRNA can be designed and produced far more efficiently and quickly.[22,23] Although siRNA delivery has made great progress, it remains a major obstacle in developing efficient siRNA-carrying vehicles for systemic delivery to distinct immune cells, for instance, macrophages.[24−26] Therefore, systemically transporting anti-CSF-1R siRNA to solid tumors and targeted delivery to M2-like TAMs with an optimal nanocarrier is a strategy with great prospects for immunotherapy.

Here, we present a molecular-targeted cancer immunotherapeutic strategy *via* dual-targeting nanoparticles delivering siRNA to M2-like TAMs. The key element of this strategy is a biocompatible fusion peptide-functionalized lipid nanoparticle with a dual-targeting entity for specific M2-like TAM binding, a sub-30 nm size for efficient penetration in solid tumor,[27,28] and stable loaded siRNA for systemic transport.[25,29] The design is illustrated in Figure 1. We speculated that SR-B1, which is highly expressed by M2-like TAMs,[30,31] would be an ideal



DOI: 10.1021/acsnano.7b05465
*ACS Nano* 2017, 11, 9536−9549

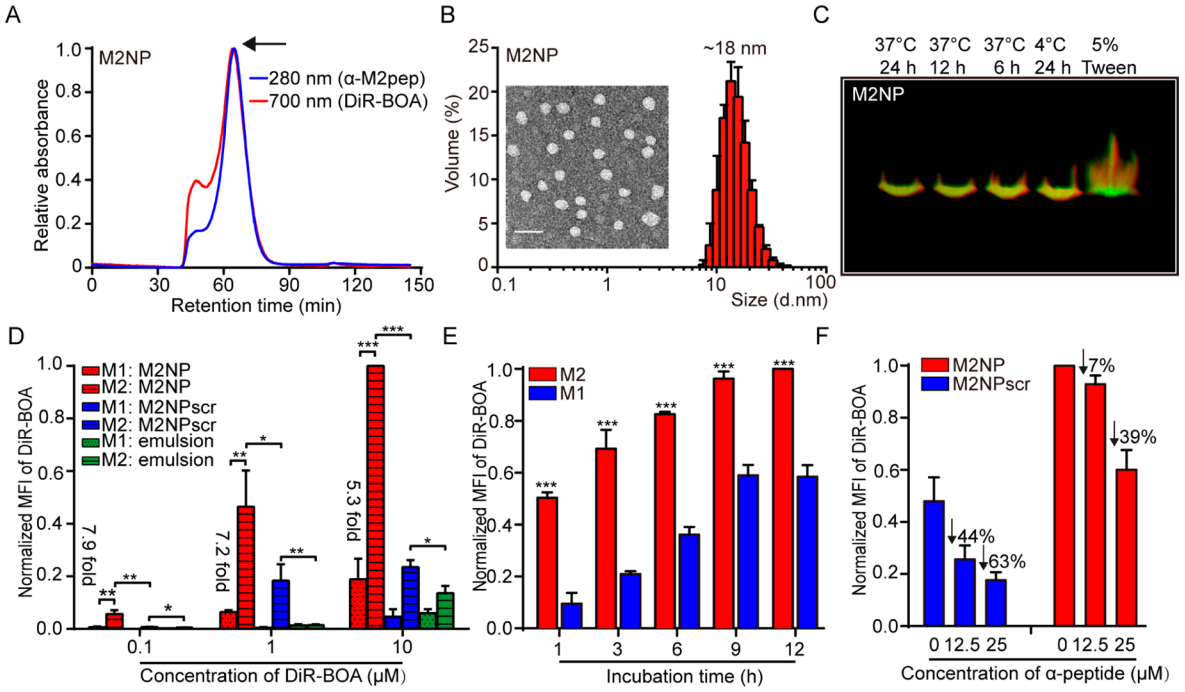


**Figure 2.** ***In vitro*** **characterization of M2NPs and evaluation of their M2 macrophage-targeting ability. (A) Representative FPLC profile of M2NPs. (B) TEM image and DLS size distribution profile of M2NPs. Scale bar: 50 nm. (C) Fluorescence image of seminative SDS-PAGE gel from the stability evaluation assay of M2NPs. Peptides on M2NPs and M2NPscrs were labeled with FITC. Green: FITC, red: DiR-BOA. (D) Comparison of M2 macrophage-targeting ability of M2NPs, M2NPscrs, and an emulsion at various concentrations. Incubation time: 1 h. MFI: mean fluorescent intensity. (E) Uptake of M2NPs by M2 and M1 macrophages at the indicated incubation time. Concentration of DiR-BOA: 10 μM. (F) Competitive inhibition experiments to evaluate the synergistic targeting effect of M2NPs to M2 macrophages. The MFI values were normalized according to the highest MFI value in (D), (E), and (F), respectively. Data are presented as the mean ± SD (two-tailed *t* test; *n* = 3).**

target for the specific binding. Exploiting the natural affinity of apolipoprotein A1 (ApoA 1) to SR-B1, we employed an ApoA 1-mimetic α-helical peptide (denoted as α-peptide) as one of the TAM-targeting units for our nanoparticle. Then, the C-terminus of α-peptide was linked with M2pep (another targeting unit) through a GSG linker to form a dual-targeting entity, designated as α-M2pep (Figure 1A). We expected that, through the amphiphilic α-peptide, α-M2pep would tightly integrate with phospholipids and core-pack (near-infrared) NiR dye to form an M2-like TAM-targeting core−shell fluorescent lipid nanoparticle, denoted as M2NP (Figure 1B). Moreover, we modified an anti-CSF-1R siRNA (siCD115)[32] with cholesterol (chol-siCD115) to mimic the endogenous delivery patterns of cholesterol by high-density lipoprotein to enhance its *in vivo* trafficking (Figure 1C).[33] With the usefulness of core NiR dye, we anticipate observing that, after intravenous injection, the M2NPs would be retained in the tumor area and efficiently target to the M2-like TAMs (Figure 1C). The M2NP would act as a powerful carrier to specifically deliver siCD115 for the blockade of the CSF-1/CSF-1R pathway in M2-like TAMs, resulting in their depletion and the activation of antitumor immune responses (Figure 1C). Therefore, with its high biocompatibility and flexibility, we expect our strategy to offer a promising platform for specific gene therapy as well as other therapeutics against TAMs.

## RESULTS

**α-M2pep Endowed the Lipid Nanoparticles with M2 Macrophage Dual-Targeting Ability.** First, we verified that α-M2pep interacted with phospholipids to form sub-30 nm nanoparticles. Films of a mixture of 1,2-dimyristoyl-*sn*-glycero-3-phosphocholine (DMPC) and cholesterol oleate (C.O) were hydrated, and the fusion peptide α-M2pep was added. For fluorescent monitoring of the uptake of nanoparticles by macrophages, DiR-BOA (an NiR fluorescent dye) was alternatively mixed with DMPC and C.O and coloaded with α-M2pep to form M2NPs (Figure 2A), which displayed uniform spherical morphology with an average diameter of ∼18 nm (Figure 2B). Importantly, the M2NPs maintained stability in 10% mouse serum at 37 °C for as long as 24 h (Figure 2C). Scrambling the sequence of M2pep (α-M2pepscr) to form control nanoparticles (M2NPscrambles, M2NPscrs) with only one targeting unit (α-peptide) had no influence on their size, morphology, and stability (Supporting Information, Figure S1A−C). In contrast, the peptide-free control (emulsion) showed a larger size and poor serum stability (Figure S1D−F).

Next, we tested the M2 macrophage targeting efficacy of M2NPs. Confocal imaging and flow cytometry data showed that both M2NPs and M2NPscrs displayed remarkably stronger (74- and 66-fold) fluorescent intensity in ldlA(mSR-B1) (SR-B1$^+$ cells) than in ldlA7 (SR-B1$^-$ cells) (Figure S2A,B). On the basis of the similar size, stability, and SR-B1 targeting ability of M2NPs and M2NPscrs, we chose to further investigate the α-peptide and M2pep in M2NPs as the key components for M2 macrophage targeting. After bone marrow-derived macrophages were cultured and polarized to either the M1 or M2 phenotype (Figure S3A,B), we compared the uptake efficiency of nanoparticles by M2 and M1 macrophages using flow cytometry. The results revealed that the uptake of M2NPs by


DOI: 10.1021/acsnano.7b05465
ACS Nano 2017, 11, 9536−9549

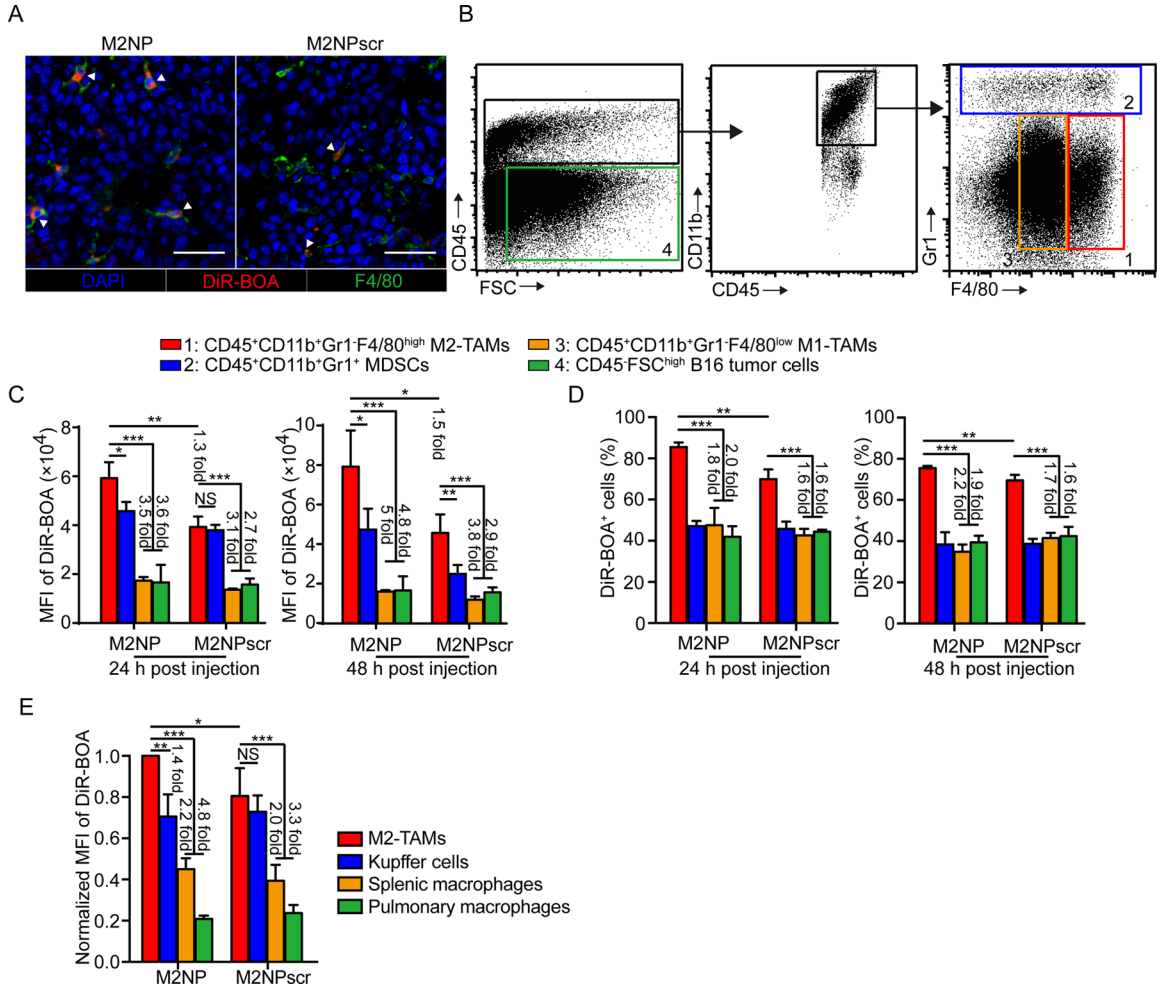


**Figure 3. Evaluation of M2-like TAM targeting by M2NPs *in vivo*. (A) Representative immunofluorescence images for the detection of F4/80$^+$ TAM targeting of M2NPs and M2NPscrs (white triangle). Blue: DAPI, red: DiR-BOA, green: Alexa Fluor 488 anti-F4/80. Scale bar: 50 $\mu$m. (B) Gating for CD45$^+$CD11b$^+$Gr1$^-$F4/80$^{high}$ M2-like TAMs (1: red box), CD45$^+$CD11b$^+$Gr1$^+$ MDSCs (2: blue box), CD45$^+$CD11b$^+$Gr1$^-$F4/80$^{low}$ M1-like TAMs (3: orange box), and CD45$^-$FSC$^{high}$ B16 cells (4: green box). (C) MFI of DiR-BOA in B16 cells, M1-like TAMs, MDSCs, and M2-like TAMs 24 and 48 h after i.v. injection ($n$ = 4 mice per group). (D) Proportions of B16 cells, M1-like TAMs, MDSCs, and M2-like TAMs that internalized M2NPs or M2NPscrs 24 and 48 h after i.v. injection ($n$ = 4 mice per group). (E) Comparison of the uptake of M2NPs by M2-like TAMs and macrophages in liver (Kupffer cells), spleen (splenic macrophages), and lung (pulmonary macrophages) at 48 h postinjection ($n$ = 4 mice per group). The MFI values of DiR-BOA were normalized according to those of the M2-like TAMs in the M2NPs administration group. Data are presented as the mean ± SD (two-tailed $t$ test).**

M2 and M1 macrophages was dose- and time-dependent (Figure 2D,E). During a 1 h incubation, M2 macrophages captured a dramatically greater amount of M2NPs than did M1 macrophages at various concentrations (7.9-, 7.2-, and 5.3-fold at 0.1, 1, and 10 $\mu$M DiR-BOA, respectively, $n$ = 3, Figure 2D). The proportion of M2 macrophages that took up M2NPs was also higher than that of M1 macrophages (3.93-, 1.38-, and 1.26-fold at 0.1, 1, and 10 $\mu$M DiR-BOA, respectively), exceeding 99% at a concentration of 10 $\mu$M (Figure S4A). As the incubation time was prolonged to 3, 6, 9, and 12 h, almost all the M1 and M2 macrophages were detected as DiR-BOA$^+$ by flow cytometry (Figure S4B). However, the uptake of M2NPs (DiR-BOA concentration: 10 $\mu$M) by M2 macrophages remained higher than that by M1 macrophages at each time point ($n$ = 3, Figure 2E). Western blot data confirmed the higher expression of SR-B1 in M2 macrophages than in M1 macrophages, which testified the potential of M2NPs for M2 macrophage targeting (Figure S5A). In addition, the M2 macrophages took up more M2NPs than M2NPscrs (7.5-, 2.5-, and 4.2-fold at 0.1, 1, and 10 $\mu$M DiR-BOA, respectively, Figure 2D), even when the DiR-BOA$^+$ cell proportion of both incubation groups exceeded 80% (10 $\mu$M DiR-BOA, Figure S4A). Moreover, the uptake of both M2NPs and M2NPscrs by M2 macrophages was dramatically higher than that of the emulsion (Figure 2D and Figure S4A). These data suggested that the two targeting units ($\alpha$-peptide and M2pep, Figure 1A) in the M2NPs had a synergistic effect on M2 macrophage targeting. To further verify this viewpoint, we performed a competitive inhibition experiment using $\alpha$-NPs that were synthesized with $\alpha$-peptide to block the SR-B1-mediated uptake in M2 macrophages.[34] The flow cytometry data showed that in M2 macrophages, as the concentration of $\alpha$-NPs increased, the internalization of M2NPscrs decreased dramatically (63% in normalized MFI and 30% in DiR-BOA$^+$ cells), whereas the reduction of the uptake of M2NPs was much lower (39% in normalized MFI and 17% in DiR-BOA$^+$ cell proportion, Figure 2F and Figure S4C). The competitive inhibition data proved that the M2 macrophage targeting of



DOI: 10.1021/acsnano.7b05465
ACS Nano 2017, 11, 9536−9549

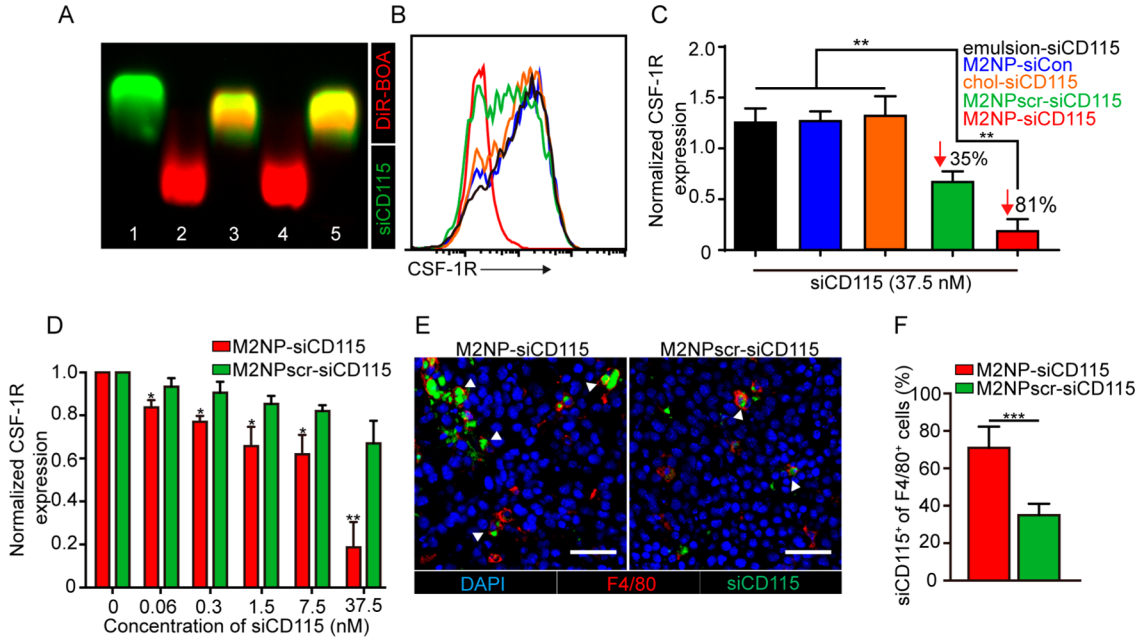


**Figure 4. Evaluation of siCD115 delivery by M2NPs and the CSF-1R inhibition by M2NP-siCD115. (A) Agarose gel electrophoresis to confirm the siCD115 loading on M2NPs. 1: free chol-siCD115; 2: M2NP; 3: M2NP-siCD115; 4: M2NPscr; 5: M2NPscr-siCD115. The siRNA was labeled with gel red (green pseudocolor). M2NP and M2NPscr were labeled with DiR-BOA (red). (B, C) CSF-1R expression on M2 macrophages respectively incubated with emulsion-siCD115, M2NP-siCon, chol-siCD115, M2NPscr-siCD115, and M2NP-siCD115 was analyzed by flow cytometry, (B) representative result, (C) quantitative data, $n$ = 3. (D) Flow cytometry data for CSF-1R expression on M2 macrophages incubated with various concentrations of M2NP-siCD115 and M2NPscr-siCD115 ($n$ = 3). (E) Immunofluorescence result to verify the delivery of siCD115 to F4/80$^+$ TAMs in B16 tumors by M2NPs. Scale bar: 50 $\mu$m. Blue: DAPI, red: Alexa Fluor 647 anti-F4/80, green: chol-siCD115-FAM. White triangle: F4/80$^+$ TAMs that internalized siCD115. (F) Quantitative results for the immunofluorescence slides shown in (E) ($n$ = 6). The CSF-1R expression was normalized according to the CSF-1R MFI value of the untreated group. Data are presented as the mean ± SD (two-tailed $t$ test).**

M2NPs resulted from the coexistence of $\alpha$-peptide and M2pep rather than the $\alpha$-peptide alone in M2NPscrs.

In addition, we tested the M2NPs' uptake of mature dendritic cells (mDCs, Figure S3C), another main phagocyte that can also be bound through SR-B1.[34] Flow cytometry data demonstrated that the affinity of M2NPs to M2 macrophages was strikingly higher than that to mDCs (Figure S6). Altogether, these data verified that M2NP was competent as an optimal dual-targeting nanoparticle for M2 macrophages and suggested its high potential for M2-like TAM binding *in vivo*.

**M2NPs Efficiently Targeted M2-like TAMs in Melanoma Tumors.** In order to investigate the TAM-targeting feasibility of M2NPs *in vivo*, M2NPs and M2NPscrs (containing 10 nmol of DiR-BOA) were injected intravenously into B16 tumor-bearing mice, respectively. As expected, the cryosection results showed that 24 h after injection, M2NPs were highly captured by F4/80$^+$ TAMs (white triangle, left panel, Figure 3A). Meanwhile, we observed visually that the fluorescent intensity of the F4/80$^+$ TAMs that took up M2NPs was obviously stronger than TAMs that took up M2NPscrs (white triangle, Figure 3A). To confirm this, we harvested tumor tissues and treated them with collagenase to obtain disaggregated cell suspensions for flow cytometry analysis, 24 or 48 h after tail vein injection. All the markers were defined according to previous reports.[18,35] The flow cytometry results showed that, at each time point, CD45$^+$CD11b$^+$Gr1$^-$F4/80$^{high}$ M2-like TAMs captured a much greater amount of M2NPs than CD45$^+$CD11b$^+$Gr1$^-$F4/80$^{int}$ M1-like TAMs (3.5−5-fold, Figure 3B,C). Moreover, excitingly, the majority of M2-like TAMs (75.5−85.4%) in the tumor microenvironment took up M2NPs (Figure 3D). Unexpectedly, the M2NPs demonstrated notable affinity to CD45$^+$CD11b$^+$Gr1$^+$ myeloid-derived suppressor cells (MDSCs) (Figure 3C), another key immunosuppressive population in the tumor region.[36] Therefore, in addition to TAMs, M2NPs might possess potential to treat MDSCs. Compared with M2NPs, the M2NPscrs group showed a lower M2-like TAM-targeting efficiency (Figure 3C,D). Meanwhile, CD45$^-$FSC$^{high}$ B16 tumor cells, the most abundant population in the tumor area, exhibited a much lower internalization of M2NPs (Figure 3C,D). Immunofluorescence staining confirmed the massive expression of SR-B1 by F4/80$^+$ TAMs (white triangle, Figure S5B) in B16 melanoma tumors, which corresponded with their M2 polarizing character and confirmed the TAM-targeting potential of M2NPs.

Next, we detected the biodistribution of M2NPs in tumors and organs of tumor-bearing mice. The results showed that at 48 h after injection, M2NPs were mainly distributed in the liver, spleen, tumor, and lung (Figure S7). Considering the presence of tissue-resident macrophages in these organs, we compared the uptake of M2NPs by Kupffer cells, splenic macrophages, M2-like TAMs, and pulmonary macrophages by flow cytometry. The data demonstrated that the fluorescence intensity of M2-like TAMs was significantly higher than that of Kupffer cells, splenic macrophages, and pulmonary macrophages (1.4-, 2.2-, and 4.8-fold, respectively), while most macrophages in these tissues displayed a considerably high DiR-BOA$^+$ proportion (Figure 3E and Figure S8A,B). Taken together, these results demonstrated the superior M2-like TAM-targeting capacity of M2NPs and revealed their potential



DOI: 10.1021/acsnano.7b05465
ACS Nano 2017, 11, 9536−9549

as an ideal nanocarrier for specific delivery of therapeutic molecules (*e.g.*, siRNA) *in vivo*.

**M2NPs Successfully Delivered siCD115 into TAMs.** We next examined the capability of M2NPs for siRNA delivery. In the tumor area, CSF-1R is specifically expressed by TAMs, and the CSF-1/CSF-1R pathway is crucial for their differentiation and survival.[21,37−39] In order to shrink the population of M2-like TAMs, we chose an anti-CSF-1R siRNA (siCD115)[32] to block the CSF-1/CSF-1R pathway. For the purpose of loading on M2NP, siCD115 was modified with cholesterol (chol-siCD115) which can insert into the lipid monolayer of M2NPs (Figure 1C). After simply mixing the chol-siCD115 with M2NPs (molar ratio: 10:1) and incubating for 1 h at room temperature, the mixture was assayed through electrophoresis to detect the loading efficiency of chol-siCD115 on M2NPs. The results showed that the band of chol-siCD115 merged ideally with the band of M2NPs (M2NPscrs as well), and free chol-siCD115 was barely detected (band 3 and band 5, Figure 4A). These data confirmed that chol-siCD115 was easily and efficiently loaded on the M2NPs (denoted as M2NP-siCD115).

Subsequently, we tested whether the M2NP-siCD115 could effectively interfere with CSF-1R expression on M2 macrophages. We verified that M2 macrophages expressed a high amount of CSF-1R, while the expression on B16 cells and M1 macrophages was quite low (Figure S9). Due to the M2-like phenotype of TAMs, there is an attractive feasibility for silencing CSF-1R using M2NP-siCD115. Flow cytometry data showed that, after 48 h of incubation, M2NP-siCD115 inhibited 81% of CSF-1R expression on M2 macrophages (Figure 4B,C). In contrast, the expression level of CSF-1R on M2 macrophages incubated with free chol-siCD115, emulsion-siCD115, or M2NP-siCon (siCon, control siRNA) did not decrease. M2NPscr-siCD115 also inhibited 35% of CSF-1R expression (Figure 4B,C), which corresponded with their lower targeting capacity for M2-like TAMs. Moreover, M2NP-siCD115 had an interference effect at a dramatically low concentration (0.06 nM, Figure 4D). These results demonstrated that with their superior M2 macrophage targeting ability, M2NPs successfully delivered siCD115 and inhibited CSF-1R expression.

To verify that siCD115 could be effectively delivered to TAMs *in vivo*, we modified the chol-siCD115 by covalently conjugating FAM (a fluorescent dye) to its 3′-terminus (denoted as chol-siCD115-FAM). Then, M2NP-siCD115-FAM were injected into the B16 tumor-bearing mice *via* the tail vein (dose of 5 mg/kg siRNA). Twelve hours after injection, the tumors were dissected for cryosectioning. The immunofluorescence results showed that M2NP-siCD115 delivered the siRNA into a higher proportion of F4/80$^+$ TAMs than did M2NPscr-siCD115 (2-fold, $n = 6$, $p < 0.001$, Figure 4E,F). Furthermore, the stronger signal of chol-siCD115-FAM in F4/80$^+$ TAMs indicated more siRNA delivered by M2NPs than by M2NPscrs (white triangle, Figure 4E). Altogether, these data indicated that M2NPs loaded with siRNA have a bright prospect for molecular-targeted tumor immunotherapy.

**M2NP-siCD115 Dramatically Inhibited Melanoma Growth and Prolonged Survival.** Finally, we evaluated the effect of M2NP-based molecular-targeted immunotherapy on B16 melanoma, a highly aggressive tumor model. M2NP-siCD115 and controls were injected through the tail vein of tumor-bearing mice, respectively (dose of 5 mg/kg siRNA), following the schedule in the time line shown in Figure 5A.

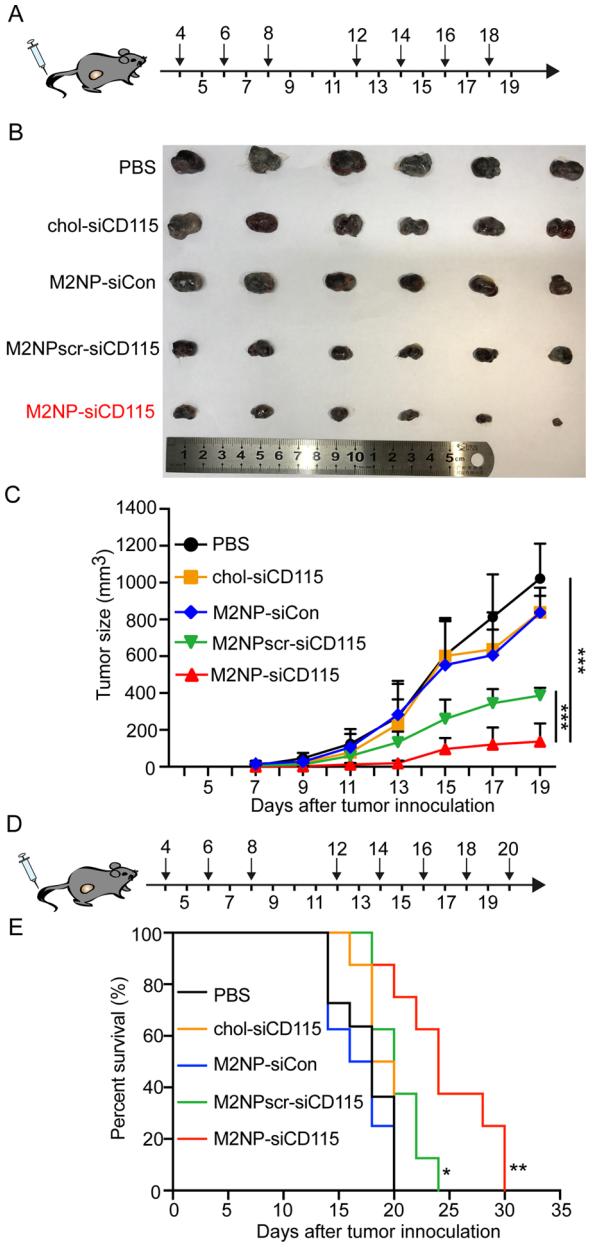


**Figure 5. Tumor growth inhibition effects of M2NP-siCD115. (A) B16 tumor treatment schedule. (B) Photograph of dissected tumor tissues from mice in different treatment groups on day 19 after tumor inoculation. (C) Tumor growth curves of B16 tumors in C57BL/6 mice treated with PBS, chol-siCD115, M2NP-siCon, M2NPscr-siCD115, or M2NP-siCD115, $n = 6$ mice per group. (D) B16 tumor treatment schedule for survival curves. (E) Survival curves of B16 tumor-bearing C57BL/6 mice treated with PBS ($n = 11$ mice), chol-siCD115, M2NP-siCon, M2NPscr-siCD115, or M2NP-siCD115 ($n = 8$ mice per group). Data are presented as the mean ± SD (two-tailed *t* test).**

Monitoring the tumor growth of the different groups showed that, after seven dose treatments, M2NP-siCD115 dramatically retarded tumor growth (Figure 5B,C). At the 19th day post tumor inoculation, compared with the phosphate-buffered saline (PBS) group, animals administrated M2NP-siCD115 showed an 87% decrease in tumor size ($P < 0.001$, $n = 6$, Figure 5C). In contrast, both the M2NP-siCon and free chol-siCD115 groups showed no significant difference in tumor size compared with the PBS group ($P > 0.05$, $n = 6$, Figure 5B,C). Meanwhile,



DOI: 10.1021/acsnano.7b05465
*ACS Nano* 2017, 11, 9536−9549

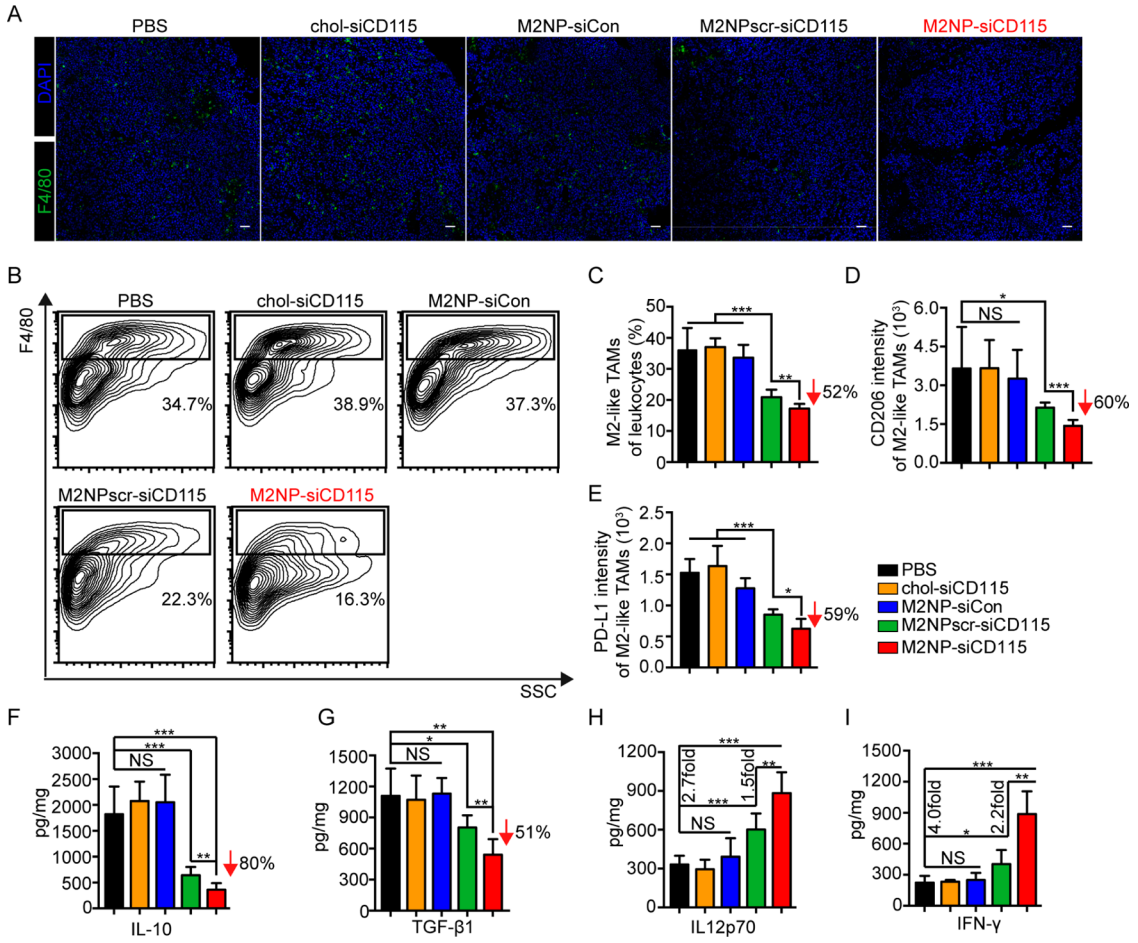


**Figure 6. M2-like TAM depletion effect and cytokine expression reprogrammed by M2NP-siCD115. (A) Representative immunofluorescence results for evaluating the presence of F4/80$^+$ TAMs after treatment with PBS, chol-siCD115, M2NP-siCon, M2NPscr-siCD115, or M2NP-siCD115. Scale bar: 50 $\mu$m. Green: Alexa Fluor 647 anti-F4/80, blue: DAPI. (B) Representative flow cytometry profile of M2-like TAMs (CD45$^+$CD11b$^+$Gr1$^-$F4/80$^{high}$) in the tumor area after the indicated treatment. (C) Proportion of M2-like TAMs among the total tumor-infiltrating leukocytes in mice after the indicated treatment, $n$ = 6 mice per group. (D) Flow cytometry data showing the CD206 expression by M2-like TAMs in tumors after the indicated treatment, $n$ = 6 mice per group. (E) PD-L1 expression on M2-like TAMs after the indicated treatment, $n$ = 6 mice per group. (F–I) ELISA results of cytokine production in the tumors from mice receiving the indicated treatment (F: IL-10; G: TGF-$\beta$1; H: IL-12p70; I: IFN-$\gamma$), $n$ = 6 mice per group. Data are presented as the mean ± SD (two-tailed $t$ test).**

the M2NPscr-siCD115 group showed less dramatic decrease in tumor size (62% decrease, $P < 0.001$, $n = 6$, Figure 5C) than that in the M2NP-siCD115 group. Moreover, M2NP-siCD115 treatment significantly prolonged the survival of the animals (Figure 5D,E). In addition, the cell cytotoxicity assay demonstrated that siRNA treatment did not directly cause tumor cell death (Figure S10). These results indicated that the tumor growth inhibition may be attributed to the activation of immune responses in the tumor microenvironment by M2NP-siCD115.

**M2NP-siCD115 Treatment Led to M2-like TAM Depletion and Reprogramed the Cytokine Secretion in the Tumor Microenvironment.** To evaluate the impact on the tumor immune environment by M2NP-siCD115 treatment, tumor tissues from each treatment group were dissected for a series of analyses. The immunofluorescence results showed that after treatment with seven doses, M2NP-siCD115 remarkably reduced the amount of F4/80$^+$ TAMs (Figure 6A). The quantitative flow cytometry results demonstrated that after M2NP-siCD115 treatment, compared with the PBS group, the M2-like TAMs (CD45$^+$CD11b$^+$Gr1$^-$F4/80$^{high}$, gating strategy is shown in Figure S11A) were decreased by 52% ($P < 0.001$, Figure 6B,C). Moreover, CD206 (a marker of M2 macrophages) expression by M2-like TAMs in the M2NP-siCD115 treatment group displayed a 60% decrease ($P < 0.001$, Figure 6D and Figure S11B). The immunohistochemistry (IHC) results also showed a decrease of F4/80$^+$CD206$^+$ TAMs after M2NP-siCD115 treatment (Figure S12). In addition, we detected a 59% decline in the expression of programmed death 1 ligand 1 (PD-L1, a T cell checkpoint molecule) on M2-like TAMs in the M2NP-siCD115 treatment group ($P < 0.001$, Figure 6E and Figure S11C). Next, we evaluated cytokine expression in the different treatment groups. As shown in Figure 6E, the enzyme-linked immunosorbent assay (ELISA) results showed that after M2NP-siCD115 treatment, the immunosuppressive IL-10 expression in the tumor was only 20% of that in the PBS group ($P < 0.001$, Figure 6F). As M2-like TAMs are the primary source of IL-10 in the tumor area,[40] the decrease in IL-10 expression was concordant with the decline in M2-like TAMs (Figure 6C,D). We also observed a 52% decrease in the expression of the immunosuppressive TGF-$\beta$1, which was expressed by immunosuppressive cells, including M2-like TAMs,[5] in tumors from the M2NP-siCD115 treatment group (Figure 6G). Together with the down-



DOI: 10.1021/acsnano.7b05465
ACS Nano 2017, 11, 9536–9549

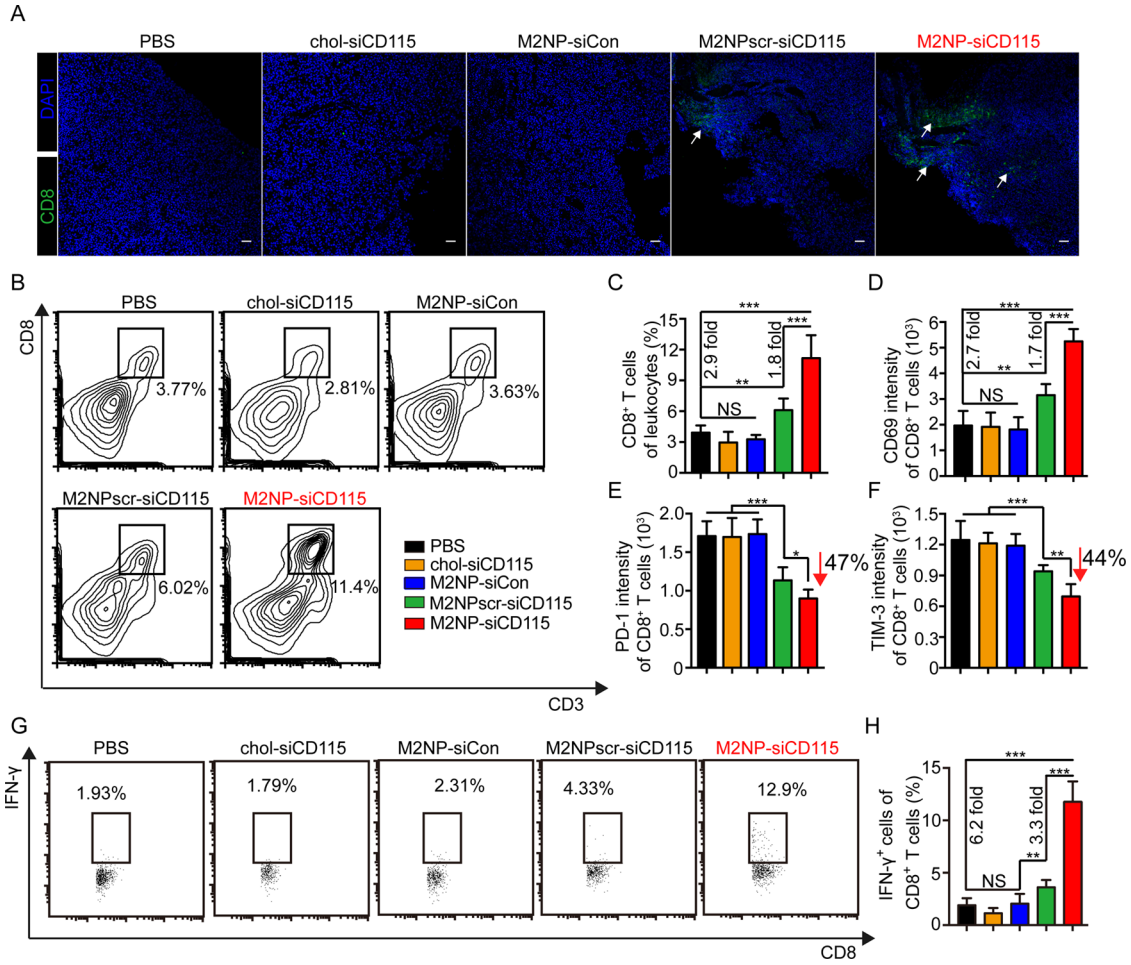


**Figure 7. Phenotypic and functional evaluation of tumor-infiltrating CD8$^+$ T cells in tumor tissues with M2NP-siCD115 treatment. (A) Representative immunofluorescence results for evaluating the presence of CD8$^+$ T cells after treatment with PBS, chol-siCD115, M2NP-siCon, M2NPscr-siCD115, or M2NP-siCD115. Scale bar: 50 $\mu$m. Green: Alexa Fluor 647 anti-CD8, blue: DAPI. (B) Representative flow cytometry profile of CD8$^+$ T cells (CD45$^+$CD3$^+$CD8$^+$) in the tumor area after the indicated treatment. (C) Proportion of CD8$^+$ T cells among the total tumor-infiltrating leukocytes in mice after the indicated treatment, $n$ = 6 mice per group. (D) Flow cytometry data showing the expression of CD69 on CD8$^+$ T cells in tumors after the indicated treatment, $n$ = 6 mice per group. (E, F) PD-1 (E) and Tim-3 (F) expression on CD8$^+$ T cells after the indicated treatment, $n$ = 6 mice per group. (G, H) IFN-$\gamma$ secretion of tumor-infiltrating CD8$^+$ T cells after the indicated treatment. (G) Representative flow cytometry profile. (H) Quantitative data, $n$ = 6 mice per group. Data are presented as the mean ± SD (two-tailed $t$ test).**

regulated IL-10 and TGF-$\beta$1 expression, we detected enhanced IL-12 expression in the M2NP-siCD115 treatment group compared with the control (PBS, chol-siCD115, and M2NP-siCon) groups ($P$ < 0.001, Figure 6H). Subsequently, in accordance with the expression of IL-12, IFN-$\gamma$ secretion in the tumor area was 4 times higher after M2NP-siCD115 treatment in comparison to the PBS group ($P$ < 0.001, Figure 6I). Meanwhile, the tumor areas treated with either chol-siCD115 or M2NP-siCon showed no significant alterations in IFN-$\gamma$ expression (Figure 6I). In addition, the increases in IL-12 and IFN-$\gamma$ expression in the M2NP-siCD115 group were notably higher than those in the M2NPscr-siCD115 group (2.2- and 1.5-fold, respectively, Figure 6H,I), supporting the importance of highly efficient M2-like TAM targeting for better siRNA treatment outcomes.

**M2NP-siCD115 Restored the Function of Infiltrating CD8$^+$ T Cells in the Tumor Microenvironment.** The up-regulation of immunostimulatory cytokines (IL-12 and IFN-$\gamma$) suggested the possibility of T cell activation; therefore, we proceeded to perform a series of analyses of the tumor-infiltrating CD8$^+$ T cells from each treatment group. Immunofluorescence staining revealed an accumulation of CD8$^+$ T cells in tumors from the M2NP-siCD115 treatment group (Figure 7A). Quantitative flow cytometry results showed that compared with the PBS group, the infiltration of CD8$^+$ T (CD45$^+$CD3$^+$CD8$^+$, the gating strategy is displayed in Figure S13A) cells elevated notably after M2NP-siCD115 administration (2.9-fold, $P$ < 0.001, Figure 7B,C), while the other control groups (chol-siCD115 and M2NP-siCon groups) showed no significant changes (Figure 7B,C). To further ensure the activation of T cells, we evaluated the surface marker expression and immune function of the tumor-infiltrating CD8$^+$ T cells in each treatment group. The results showed that the M2NP-siCD115 administration significantly up-regulated CD69 (a T cell activation marker) expression on CD8$^+$ T cells in tumors (2.7-fold compared with the PBS group, $P$ < 0.001, Figure 7D and Figure S13B). In addition, the expression levels of PD-1 and Tim-3 (T cell exhaustion markers)[41] were both decreased after M2NP-siCD115 treatment (47% for PD-1 and 44% for Tim-3, compared with the PBS group, $P$ < 0.001,


DOI: 10.1021/acsnano.7b05465
ACS Nano 2017, 11, 9536−9549

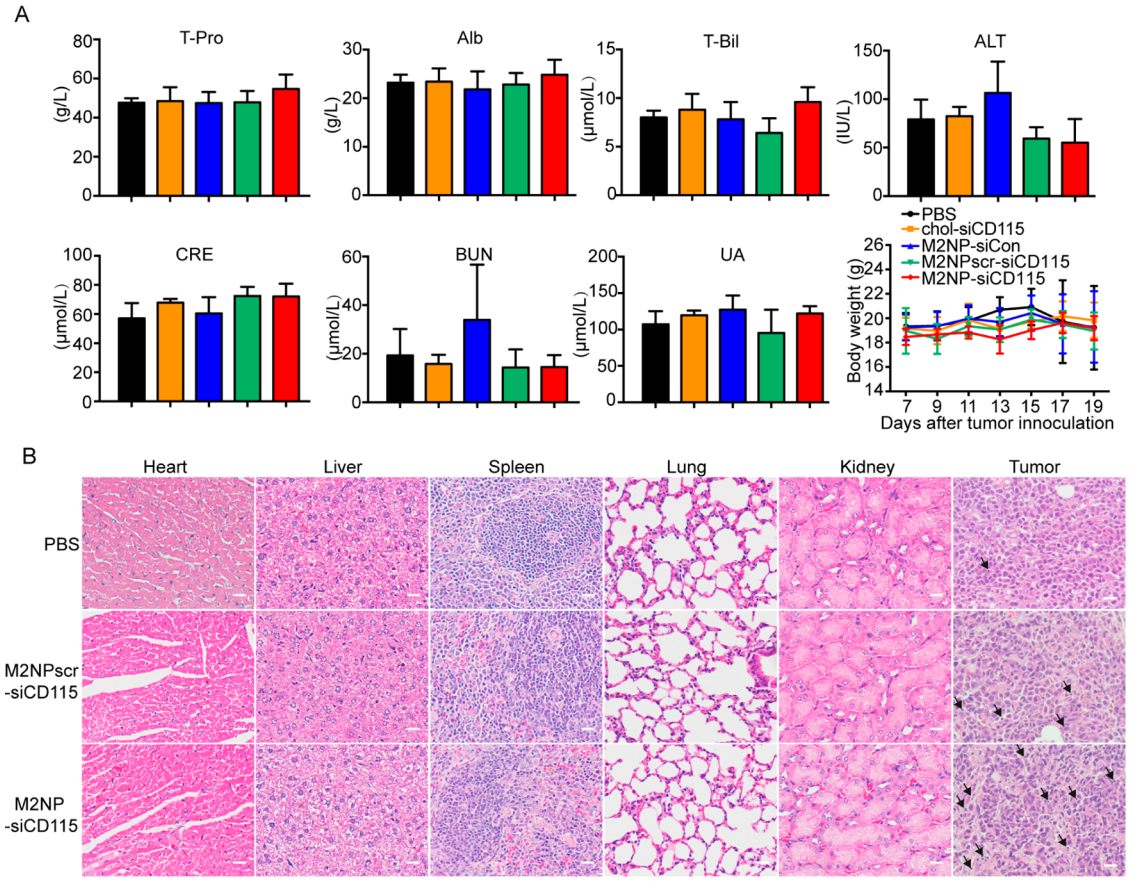


**Figure 8. Biosafety evaluation of M2NP-siCD115 *in vivo*. (A) Biochemical analysis and body weight monitoring of tumor-bearing mice treated with PBS, chol-siCD115, M2NP-siCon, M2NPscr-siCD115, or M2NP-siCD115 (T-Pro: total protein; ALB: albumin; T-Bil: total bilirubin; ALT: alanine aminotransferase; CRE: creatinine; BUN: urea nitrogen; UA: uric acid). (B) Histopathologic analyses of H&E-stained tissue sections from heart, liver, spleen, lung, kidney, and tumors of tumor-bearing mice after the indicated treatment, scale bar: 20 μm. Black arrow: tumor-infiltrating leukocytes.**

Figure 7E,F and Figure S13B), while no significant difference was detected for CTLA-4 expression in either group (Figure S13B,C). Then, flow cytometry data demonstrated that the IFN-$\gamma$ secretion by $CD8^+$ T cells was dramatically increased in the M2NP-siCD115 treatment group (6.2-fold, compared with the PBS group, $P < 0.001$, Figure 7G,H and Figure S14). In addition, these results showed that M2NP-siCD115 had a more positive impact than M2NPscr-siCD115 on the activation and function of the tumor-infiltrating $CD8^+$ T cells (Figure 7), which emphasized the superiority of M2NPs for the M2-like TAM targeting.

**M2NP-siCD115 Treatment Showed Superior Biocompatibility.** After the tumor inhibition experiment, we collected blood and organ samples (heart, liver, spleen, lung, and kidney) from mice for biosafety evaluation. The biochemical analysis results showed that, between the treatment (M2NP-siCD115 and M2NPscr-siCD115) and control (PBS, chol-siCD115 and M2NP-siCon) groups, no significant differences were detected in the hepatic and renal function parameters (total protein (T-Pro), albumin (ALB), total bilirubin (T-Bil), alanine aminotransferase (ALT), creatinine (CRE), urea nitrogen (BUN), and uric acid (UA)) (Figure 8A). Moreover, compared with the PBS group, the organ samples in the M2NPscr-siCD115 and M2NP-siCD115 treatment groups showed no histopathological abnormities or lesions (Figure 8B). The IHC results showed no apparent changes in the presence of $F4/80^+$ macrophages and their levels of CD206 expression in liver, spleen, and lung after M2NP-siCD115 treatment (Figure S12). In addition, the H&E staining results showed enhanced leukocyte infiltration in tumors after M2NP-siCD115 treatment (Figure 8B). Together with the body weight monitoring, these results indicated superior biocompatibility of M2NP-siCD115.

Altogether, these results revealed the notable biocompatibility and effectiveness of M2NP-siCD115 as a potent molecular-targeted immunotherapy for specifically depleting M2-like TAMs, restoring the immune function of tumor-infiltrating $CD8^+$ T cells, and suppressing the growth of melanoma tumors *in vivo*.

## DISCUSSION

M2-like TAMs are regarded as an appealing therapeutic target because of their numerous pro-tumor characteristics.[5] In this study, we reported a molecular-targeted strategy based on unique dual-targeting nanoparticles, denoted as M2NPs. With the superior affinity for M2-like TAMs in melanoma, M2NPs delivered the anti-CSF-1R siRNA (siCD115) to their cytoplasm in a highly efficient manner (Figure 4E). The M2NP-based successful siRNA delivery resulted in a proportional decrease in M2-like TAMs (52%), inhibition of tumor growth (87%), and prolonged survival and restored the T cell immune function in the tumor microenvironment.

The whole-body distribution and the heterogeneity resulting from the polarization difference (M1 and M2) of macrophages



DOI: 10.1021/acsnano.7b05465
*ACS Nano* 2017, 11, 9536−9549

make the M2-like TAM-targeted drug delivery a crucial and challenging issue.[5,8,18,42,43] Here, we developed M2-like TAM dual-targeting nanoparticles and first determined that SR-B1 is an ideal receptor for their specific targeting. α-M2pep, the dual-targeting entity of M2NPs, was produced by linking α-peptide (an SR-B1 targeting peptide) with M2pep (Figure 1A). The M2pep had been shown as a promising M2-like TAM-binding peptide and applied on a TAM-targeting nanoparticle in previous studies.[18,44] In our case, M2NPs exhibited superior targeting efficiency to both M2 macrophages (*in vitro*) and M2-like TAMs (*in vivo*), which was better than that of M2NPscrs (control nanoparticles with one targeting unit) (Figures 2D and 3C,D). The competitive inhibition experiment confirmed that the α-peptide and M2pep (two targeting units in α-M2pep) functioned synergistically for the specific M2 macrophage binding of M2NPs (Figure 2F). In our previous work, we successfully targeting delivered antigens to mDCs through SR-B1.[34] Compared with mDCs, M2 macrophages captured a much higher amount of M2NPs (Figure S6), which might mainly result from the synergistic targeting effect of M2NPs besides a possible difference in SR-B1 expression. In addition, when targeting to M2-like TAMs in melanoma, M2NPs moderately bound to tumor cells (Figure 3C,D). On the contrary, in the study of Cieslewicz *et al.*, the tumor cells took up an even higher amount of M2pep than M2-like TAMs.[18] These inconsistent results indicate the superiority of our dual-targeting strategy.

The biodistribution measurement showed that M2NPs had a higher accumulation in organs such as liver and spleen than in tumors (Figure S7). However, the flow cytometry analysis demonstrated a higher affinity of M2NPs for M2-like TAMs compared with other tissue-resident macrophages (Kupffer cells, splenic macrophages, and pulmonary macrophages, Figure 3E and Figure S8A−C). Considering that the tissue-resident macrophages were shaped by the local microenvironment, we speculated that the TAMs were more polarized toward an M2 phenotype than other macrophages.[45] The IHC results demonstrated an obvious difference in morphology and CD206 expression between TAMs and tissue-resident macrophages in normal tissues (*e.g.*, liver, spleen, and lung), which supported the differences in polarization between these macrophage populations (left line in Figure S12). These results provide strong support for the targeting ability of M2NPs to M2-like TAMs. Besides, though lower than M2-like TAMs, the uptake of M2NPs by Kupffer cells was higher than macrophages in the spleen and lung (Figure 3E). This may result from the accumulation of M2NPs in the liver (Figure S7) and the SR-B1 expression and strong phagocytic ability of the Kupffer cells.[46,47] Meanwhile, compared with TAMs, the CSF-1R (CD115) expression levels of tissue-resident macrophages (Kupffer cells, splenic macrophages, and pulmonary macrophages) are quite low.[20,48−50] Even captured by these macrophages, the M2NP-siCD115 would have a very limited effect on them. Thus, the M2-like TAM-targeting ability, combined with the CSF-1R targeted therapy, led to the specific M2-like TAM depletion and low immunotoxicity of M2NP-siCD115.

Previously, Conde *et al.* reported a promising strategy for the targeted delivery of anti-VEGF siRNA to both tumor cells and TAMs, which effectively depleted TAMs and slowed tumor growth at a notable low dose.[44] However, considering that their anti-VEGF strategy resulted in the death of tumor cells and TAMs simultaneously, and to more specifically deplete TAMs and reverse the associated immunosuppressive environment, an optimal molecule target should be considered.

CSF-1R, which is mainly expressed by macrophages and monocytes (macrophage precursor), is essential for their differentiation and survival. Moreover, experimental data from ourselves (Figure S9) and other researchers confirmed that M2 macrophages expressed a higher amount of CSF-1R than M1 macrophages.[42] Thus, CSF-1R-targeted treatment is highly M2-like TAM specific.[22,42] Instead of the extensively utilized small molecular drugs and antibodies, we focused on the rarely studied gene therapy to block CSF-1R due to the ease of siRNA modification and production. The siCD115 reported by Dutta *et al.*[32] was first employed in cancer therapy by us through modification with cholesterol for their loading on M2NPs (Figure 1C). Through specific delivery, M2NP-siCD115 efficiently blocked CSF-1R expression in M2 macrophages and depleted M2-like TAMs in the tumor region (Figure 4B−D, Figure 6B,C). In addition, the administration of M2NP-siCD115 led to a dramatic inhibition of immunosuppressive cytokine (IL-10 and TGF-β) expression but a notable increase in $CD8^+$ T cell infiltration and immunostimulatory cytokine (IL-12 and IFN-γ) secretion in the tumor area (Figure 6F−I). More importantly, after treatment, the T cell exhaustion markers (*e.g.*, PD-1 and Tim-3) were significantly down-regulated, while the function (CD69 expression and IFN-γ production) of these infiltrating $CD8^+$ T cells dramatically recovered (Figure 7D−H). However, Zhu *et al.* reported that, after CSF-1/CSF-1R blockade with a small-molecule inhibitor, the PD-1 expression level remained unchanged on $CD8^+$ T cells in pancreatic ductal adenocarcinoma tumor.[39] We speculated that the different delivery and uptake pathways of the drugs in these studies might underlie the distinct CSF-1R inhibition efficiencies and activation of the immune environment in the tumor through different mechanisms. Meanwhile, the different tumor models used in these studies should also be considered. Thus, these discordant results were reasonable.

The combination of immunotherapy with traditional treatments, such as chemotherapy or radiotherapy, is an emerging trend in cancer therapy.[51] For example, the combination of low-dose cyclophosphamide and T cell adoptive transfer therapy produced a better therapeutic effect.[52] Similarly, M2NP-siCD115 can also be combined with other treatments. For instance, during chemotherapy, M2NP-siCD115 can be used for eliminating chemoresistance caused by M2-like TAMs. Besides M2-like TAMs, M2NPs showed considerable affinity for MDSCs, which revealed their potential for broad-spectrum targeting to immunosuppressive cells in tumors. Through altering the loaded drugs, M2NPs may possess the capacity to treat TAMs and MDSCs simultaneously. Furthermore, with the dual-targeting ability, M2NPs may act as potent carriers to deliver various drugs for treatments of other diseases involving M2-like macrophages, such as asthma and atherosclerosis.[10,53] Considering the promising use of M2NP, in a future study, it will be attractive to employ more siRNA of immunosuppressive molecules related to M2-like TAMs or MDSCs on M2NPs to expand the molecular-targeted strategy. For instance, simultaneous delivery of anti-PD-L1 siRNA to M2-like TAMs and MDSCs through M2NPs may block T cell apoptosis and enhance their activation.[54,55] In addition, more work should be done to lower the siRNA dose for wider application of our molecular-targeted strategy.



DOI: 10.1021/acsnano.7b05465
*ACS Nano* 2017, 11, 9536−9549

## CONCLUSION

In general, we developed a superior nanocarrier, M2NP, with dual-targeting capability for M2-like TAMs. Through a molecular-targeted strategy based on M2NPs, anti-CSF-1R siRNA (siCD115) was efficiently delivered to M2-like TAMs, leading to a dramatic reduction in TAMs, reversing tumor immune suppression and, finally, inhibiting melanoma tumor growth. Our study emphasizes the importance of multiligands for the binding of heterogeneous TAMs, enriches the TAM-targeting strategies, and extends the treatment approaches for malignant tumors, such as melanoma.

## METHODS

**Materials.** Cholesterol oleate, Hoechst 33258, and protease inhibitor cocktail were purchased from Sigma-Aldrich Co. (St. Louis, MO, USA). 1,2-Dimyristoyl-*sn*-glycero-3-phosphocholine and 1,2-distearoyl-*sn*-glycero-3-phosphoethanolamine-*N*-(amino(polyethylene glycol)-2000) (DSPE-PEG2000) were obtained from Avanti Polar Lipids Inc. (Alabaster, AL, USA). α-M2pep (Ac-FAEKFKEAVK-DYFAKFWD-GSG-YEQDPWGVKWWY) and α-M2pepscr (Ac-FAEKFKEAVKDYFAKFWD-GSG-WEDYQWPVYKGW) were synthesized by Bankpeptide Ltd. (Hefei, China). All siRNA were synthesized by Genepharma Co. (Shanghai, China). The CSF-1R-targeted cholesterol-conjugated siRNA (cholesterol-siCD115, abbreviation: chol-siCD115) consisted of the sense strand 5′-chol-cuAcucAAcuuucuccGAA-dTsdT-3′ and antisense strand 5′-UUCGGAGAAAGUUGAGuAG-dTsdT-3′. The negative control cholesterol-conjugated siRNA (cholesterol-siCon, abbreviation: chol-siCon) consisted of the sense 5′-chol-UUCUCCGAACGUG-UCACGUTT-dTsdT-3′ and antisense strand 5′-ACGUGACA-CGUUCGGAGAATT-dTsdT-3′. The lowercase letters identify 2′Ome-modified nucleotides.

**Mice and Cells.** Female C57BL/6 mice (8−12 weeks old) were purchased from HFK Bioscience (Beijing, China). All of the mice were maintained under a specific pathogen-free barrier facility at Animal Center of Wuhan National Laboratory for Optoelectronics. All animal studies were conducted in compliance with protocols that had been approved by the Hubei Provincial Animal Care and Use Committee and in compliance with the experimental guidelines of the Animal Experimentation Ethics Committee of Huazhong University of Science and Technology. The B16F10 cells (purchased from the BOSTER Company, Wuhan, China) were cultured in RPMI-1640 medium containing 10% fetal bovine serum (FBS) and 100 U/mL penicillin−streptomycin. The ldlA7 and ldlA(mSR-B1) cell lines were kindly provided by Dr. Monty Krieger (Massachusetts Institute of Technology, Cambridge, MA, USA). The two cell lines were cultured in similar medium (Hams F-12 media with 2 mM L-glutamine, 100 U/mL penicillin−streptomycin, and 5% FBS) with (ldlA(mSR-B1)) or without (ldlA7) 300 mg/mL geneticin. All cells were cultured under 5% $CO_2$ at 37 °C in an incubator (Thermo, USA).

**Synthesis of M2NP.** The M2NPs were synthesized as follows. (1) A mixture of 15 μmol of DMPC, 0.057 μmol of DSPE-PEG2000, 1 μmol of DiR-BOA (1,10-dioctadecyl-3,3,30,30-tetramethylindotricarbocyanine iodide bis-oleate), and 0.5 μmol C.O in chloroform was dried with nitrogen to form a uniform film. (2) Then, for hydration, 5 mL of PBS solution was added to the dried film and vortexed for 5 min. Subsequently, the mixture was sonicated for 1 h at 48 °C. (3) α-M2pep (or α-M2pepscr) peptide (8 mg) was dissolved in 8 mL of PBS, added dropwise to the lipid emulsion, and then stored overnight at 4 °C. After concentration using centrifugal filter units (30 Kd, Millipore, USA), the nanoparticles were purified using the Akta fast protein liquid chromatography (FPLC) system with a HiLoad 16/60 Superdex 200 pg column (General Electric Healthcare, NY, USA). The peptide concentration was measured using a CBQCA protein quantitation kit (Invitrogen Corporation, CA, USA). The lipid concentration was determined by a phospholipid C assay kit (Wako Pure Chemical, Japan). The molar concentration of M2NPs ($C_{M2NP}$) was determined according to the previously reported method.[56] Chol-siRNA (chol-siCD115) was dissolved in RNase-free water and mixed with M2NP solution at a molar ratio of 10:1 for 1 h at room temperature. Then, the integrity of resulting M2NP-siCD115 was verified by fluorescence imaging after agarose gel electrophoresis.

**Stability Evaluation of Nanoparticles.** The stability of the nanoparticles was evaluated using seminative SDS-polyacrylamide gel electrophoresis (SDS-PAGE). The peptides on M2NPs and M2NPscrs were labeled with FITC. FITC-M2NPs, emulsion, and FITC-M2NPscrs were loaded on 8% seminative SDS-PAGE gels after incubation with 10% mice serum for 6−24 h at 37 °C. Then, the bands were detected by fluorescence imaging. FITC-M2NPs incubated at 4 °C or with Tween-20 were used as controls.

**Generation of Bone Marrow-Derived Macrophages (BMDMs) and Bone Marrow-Derived Dendritic Cells (BMDCs).** The femurs and tibias of 8−10 weeks old C57BL/6 mice were aseptically dissected and flushed with a syringe to obtain bone marrow (BM) cells. To prepare BMDMs, BM cells were cultured in complete DMEM medium (10% FBS, 1% sodium pyruvate, 1% nonessential amino acids, 50 μM β-mercaptoethanol, 100 U/mL penicillin−streptomycin, and 20 ng/mL recombinant mouse M-CSF (PeproTech)) and seeded at a concentration of $1 \times 10^6$ cells/mL in six-well tissue culture plates. The medium was half-replaced on the third day. On day 6, to induce polarization, the BMDMs were incubated for 48 h in medium with different cytokines as follows: IFN-γ (PeproTech, 20 ng/mL) and LPS (100 ng/mL) for M1 macrophages and IL-4 (PeproTech, 20 ng/mL) for M2 macrophages. The polarization of M1 and M2 macrophages was confirmed by detecting specific markers (F4/80, CD206, CD86, and MHC-II) by flow cytometry.[57] To generate BMDCs, BM cells were cultured in RPMI-1640 medium containing 10% FBS, 1% sodium pyruvate, 1% nonessential amino acids, 50 μM β-mercaptoethanol, 100 U/mL penicillin−streptomycin, 10 ng/mL recombinant mouse GM-CSF (PeproTech), and 1 ng/mL IL-4 (PeproTech). On day 6, the immature DCs were induced to mature with 1 μg/mL LPS for 24 h. Antibodies against maturation markers of DCs, such as anti-CD11c (clone N418), anti-CD80 (clone 16-10A1), anti-CD86 (clone GL-1), anti-MHC-II (clone 11-5.2), and anti-CD205 (clone NLDC 145), were used to ensure that mDCs were successfully obtained.[34,58]

**Western Blotting.** After harvesting M1 and M2 macrophages, the cells were lysed with RIPA lysis buffer (Beyotime, China) and centrifuged at 12 000 rpm for 5 min at 4 °C. The supernatants were collected and loaded on SDS-PAGE. Western blotting for SR-B1 was performed with rabbit anti-SR-B1 antibody (1:10 000; Novus, catalogue number NB-400-104, USA) and horseradish peroxidase (HRP)-conjugated anti-rabbit secondary antibody (1:2000; ProteinTech, catalogue number SA00001-2, Wuhan, China). β-Actin was detected with mouse anti-β-actin antibody (1:2000; ProteinTech, clone 7D2C10, Wuhan, China) and HRP-conjugated anti-mouse secondary antibody (1:2000; ProteinTech, catalogue number SA00001-1, Wuhan, China). The ldlA7 and ldlA(mSR-B1) cells were used as negative and positive controls, respectively.

**Confocal Imaging.** To evaluate the SR-B1-targeting ability of M2NPs, M2NPscrs, and emulsion, ldlA7 ($SR\text{-}B1^-$) and ldlA(mSR-B1) ($SR\text{-}B1^+$) cells were seeded in eight-well cover-glass-bottom chambers (Nunc Lab-Tek, Sigma-Aldrich) ($5 \times 10^4$/well) and incubated with M2NPs, M2NPscrs, and emulsion (DiR-BOA, 10 μM) for 1 h, respectively. Then, 15 min before three washings, Hoechst 33258 (0.5 μg/mL) was added. The fluorescent images were acquired using LSM 710 laser confocal scanning microscopy (Zeiss, Germany) with an excitation wavelength of 405 nm for Hoechst 33258 and 633 nm for DiR-BOA.

**Flow Cytometry Analysis.** To quantify the SR-B1-targeting efficiency, ldlA7 ($SR\text{-}B1^-$) and ldlA(mSR-B1) ($SR\text{-}B1^+$) were incubated with M2NPs, M2NPscrs, and emulsion (DiR-BOA, 10 μM) for 1 h, respectively. Then, the cells were washed with PBS and loaded for flow cytometry analysis. For M2 macrophage-targeting detection, M1 and M2 macrophages were incubated with M2NPs, M2NPscrs, and emulsion at various concentrations for 1−12 h. All the cells were analyzed using a CytoFLEX flow cytometer (Beckman



DOI: 10.1021/acsnano.7b05465
ACS Nano 2017, 11, 9536−9549

Coulter, USA). The data were analyzed using FlowJo software (FlowJo, Ashland, OR, USA).

**Biodistribution Analysis of M2NPs.** Organs (liver, spleen, heart, kidney, lung, and brain) and tumor tissues were harvested from mice 48 h postinjection of M2NPs or M2NPscrs. Samples were weighed and homogenized in PBS. Homogenates were then extracted using a 3-fold excess of chloroform/methanol (2:1). The fluorescence of the tissue extracts was measured (excitation: 750 nm; emission: 810 nm) and presented as the fluorescence intensity per mg of tissue.

**Evaluation of the Uptake of M2NPs by Tissue-Resident Macrophages.** Briefly, mice were perfused with EGTA/HBSS and collagenase solution *via* the portal vein. Then, liver, spleen, and lung were dissected to obtain single-cell suspensions. Specifically, to collect nonparenchymal cells of liver, the resulting suspensions were centrifuged at 1260 *g* for 15 min in 30% and 50% Percoll solution. The samples were then stained with antibodies and analyzed by flow cytometry using gating strategies described in a previous report ($CD45^+F4/80^{high}CD11b^{mid}$ for Kupffer cells, splenic macrophages, and pulmonary macrophages).[59]

**siRNA Inhibition.** M2 macrophages were incubated with emulsion-siCD115, chol-siCD115, M2NP-siCon, M2NPscr-siCD115, and M2NP-siCD115 in the 24-well tissue culture plates (siCD115 concentration, 37.5 nM), respectively. Furthermore, M2NP-siCD115 and M2NPscr-siCD115 were tested for a CSF-1R expression interfering effect at concentrations of 0.06, 0.3, 1.5, 7.5, and 37.5 nM. After 48 h of incubation, the resulting cells were labeled with anti-CD115 antibody (clone AFS98 BioLegend, San Diego, CA, USA) for flow cytometry analysis using a CytoFLEX flow cytometer (Beckman Coulter, USA). The data were analyzed using FlowJo software.

**Tumor Growth Inhibition.** C57BL/6 mice were randomly divided into 5 groups and anesthetized with isoflurane; then, $5 \times 10^4$ B16F10 cells were transplanted subcutaneously into the right flank of the mice. Four days after tumor inoculation, the mice were intravenously injected with M2NP-siCD115, M2NPscr-CD115, chol-siCD115, M2NP-siCon, and PBS on days 4, 6, 8, 12, 14, 16, and 18 with a dose of 5 mg/kg (siCD115). Tumors were measured using digital calipers, and the tumor volume ($mm^3$) was calculated as $(A \times B^2)/2$, where $A$ and $B$ represent the length and width of the tumor, respectively. Body weight of the mice was recorded while measuring the tumor size.

**Analysis of Tumor-Infiltrating Leukocytes.** After sacrificing the tumor-bearing mice, B16 tumors were dissected and cut into pieces with a scissors before incubated with a cocktail of enzymes dissolved in RPMI-1640 medium (1 mg/mL collagenase, Worthington; 0.1 mg/mL DNase I, Sigma-Aldrich) for 30 min at 37 °C. The homogenates were then washed and passed through a 70 $\mu$m nylon mesh to acquire single-cell suspensions. A live/dead fixable aqua dead cell stain kit (Invitrogen, Carlsbad, CA, USA) was used to remove dead cells. Subsequently, the suspensions were divided into two parts for TAM and T cell detection. A total number of $\sim 1.5 \times 10^6$ cells were analyzed for every sample from each treatment group. Antibodies against CD45 (clone 30-F11), CD11b (clone M1/70), Gr1 (clone RB6-8C5), F4/80 (clone BM8), PD-L1 (clone 10F.9G2), and CD206 (clone C068C2) were used to detect TAMs and MDSCs, while anti-CD45, anti-CD3 (clone 17A2), anti-CD8 (clone 53-6.7), anti-CD69 (clone H1.2F3), anti-PD-1 (clone RMP1-14), anti-CTLA-4 (clone UC10-4B9), anti-Tim-3 (clone RMT3-23), and anti-IFN-$\gamma$ (clone XMG1.2) antibodies were added for T cell detection. All the antibodies were purchased from BioLegend. All the cells were analyzed by the CytoFLEX flow cytometer (Beckman Coulter, USA). The data were analyzed using FlowJo software.

**Evaluation of IFN-$\gamma$ Secretion by Tumor-Infiltrating $CD8^+$ T Cells.** For detecting the intracellular IFN-$\gamma$ in $CD8^+$ T cells in tumors, the tumor-infiltrating lymphocytes (TILs) were isolated. In brief, tumor tissues were minced and further dissociated with collagenase IV and DNase I. Cell suspensions were passed through a 70 $\mu$m cell strainer and centrifuged. The resulting cell pellets were resuspended in 40% Percoll and overlaid onto 80% Percoll and centrifuged for 20 min at 4 °C. TILs were collected from the interface between the discontinuous Percoll gradient. The TILs were then seeded in 24-well culture plates and supplemented with 30 $\mu$g/mL whole tumor antigen, cell activation cocktail (BioLegend), and brefeldin A for 8 h. Finally, the cells were collected and stained with anti-CD3 and anti-CD8 antibodies before intracellular staining for IFN-$\gamma$. The data were analyzed using FlowJo software.

**ELISA Assay.** B16 tumors were harvested, and their mass was measured. Then, samples were homogenized on ice in PBS containing protease inhibitor cocktail (Sigma-Aldrich). After centrifuging at 12 000 rpm for 5 min at 4 °C, the resultant supernatants were collected for detection of IL-10, IL-12p70, TGF-$\beta$1, and IFN-$\gamma$ with ELISA kits according to the manufacturer's instruction (Dakewe, China).

**Immunofluorescence Staining.** For the immunofluorescence analysis, tumor tissues were fixed in 4% paraformaldehyde for 12 h at 4 °C and then dehydrated in 30% sucrose solution. The tissues were then frozen in OCT (Sakura, Torrance, CA, USA) compound and sectioned into 10 $\mu$m slices using a freezing microtome (Leica, Germany). OCT was removed by washing three times in PBS, and the sections were immunostained with Alexa Fluor 488 anti-mouse F4/80 (BioLegend, clone BM8) or Alexa Fluor 647 anti-mouse F4/80 (clone BM8) for the TAM detection. To identify SR-B1, the slices were immunostained with rabbit anti-SR-B1 antibody (Novus, USA) and then labeled with goat anti-rabbit IgG (H+L) conjugated to Alexa Fluor 647 (Invitrogen, USA). All the sections were imaged with LSM 710 laser confocal scanning microscopy (Zeiss, Germany). The data were analyzed using ImageJ software.

**Biochemical and Histopathological Analysis.** On the 19th day of tumor inoculation, mice blood was collected and analyzed using an automatic biochemical analyzer (Spotchem EZ SP-4430, Arkray Inc., Kyoto, Japan). The detected hepatic and renal function parameters were as follows: total protein, albumin, total bilirubin, alanine aminotransferase, creatinine, urea nitrogen, and uric acid. The hearts, livers, spleens, lungs, and kidneys were harvested from tumor-bearing mice and fixed in 4% paraformaldehyde solution. Then the organs were embedded in paraffin, sectioned, and processed for hematoxylin and eosin (HE) staining. The HE sections were imaged on a Nikon Ni-E (Nikon, Minato, Tokyo, Japan). All images were acquired with NIS-Elements software and further analyzed with ImageJ.

**Statistical Analysis.** Statistical analysis was performed using GraphPad Prism 6 (GraphPad Software, CA, USA). For comparisons of two groups, the two-tailed unpaired $t$ test was performed. Survival data were analyzed using the Kaplan–Meier method. Significant differences between or among the groups are indicated by NS for no significant difference, * for $P < 0.05$, ** for $P < 0.01$, and *** for $P < 0.001$.

## ASSOCIATED CONTENT

### Supporting Information

The Supporting Information is available free of charge on the ACS Publications website at DOI: 10.1021/acsnano.7b05465.

Additional data of the characterization of M2NPscr and emulsion, SR-B1 targeting ability of M2NPs, gating strategies of BMDCs, BMDMs, M2-like TAMs, tissue resident macrophages, and $CD8^+$T cells, SR-B1 expression of M2 macrophages and TAMs, biodistribution measurement of M2NPs, CSF-1R expression on B16, M1, and M2 macrophages, IHC analysis of macrophages in different tissues (PDF)

## AUTHOR INFORMATION

### Corresponding Author

*E-mail (Z. Zhang): czyzzh@mail.hust.edu.cn.

### ORCID

Yuan Qian: 0000-0002-3967-7727

Zhihong Zhang: 0000-0001-5227-8926



DOI: 10.1021/acsnano.7b05465
*ACS Nano* 2017, 11, 9536–9549

### Author Contributions

[§]Y. Qian and S. Qiao contributed equally.

### Notes

The authors declare no competing financial interest.

## ACKNOWLEDGMENTS

We thank Dr. Gang Zheng (University of Toronto, Toronto, ON, Canada) for paper discussion and Dr. Monty Krieger of MIT for providing ldlA7 and ldlA(mSR-B1) cell lines. We also thank the Optical Bioimaging Core Facility of WNLO-HUST for the support in data acquisition, the Center for Nanoscale Characterization & Devices (CNCD, Tecnai G2 20 U-Twin) in WNLO-HUST for the facility support, and the Analytical and Testing Center of HUST for spectral measurements. This work was supported by the Major Research plan of the National Natural Science Foundation of China (Grant No. 91442201), National Science Fund for Distinguished Young Scholars (Grant No. 81625012), Science Fund for Creative Research Groups of the National Natural Science Foundation of China (Grant No. 61421064), the Fundamental Research Funds for the Central Universities (HUST: 2015ZDTD014), and the Director Fund of WNLO.

## REFERENCES

(1) Wagle, N.; Emery, C.; Berger, M. F.; Davis, M. J.; Sawyer, A.; Pochanard, P.; Kehoe, S. M.; Johannessen, C. M.; Macconaill, L. E.; Hahn, W. C.; Meyerson, M.; Garraway, L. A. Dissecting Therapeutic Resistance to RAF Inhibition in Melanoma by Tumor Genomic Profiling. *J. Clin. Oncol.* **2011**, *29*, 3085−3096.

(2) Early Breast Cancer Trialists' Collaborative Group (EBCTCG): Darby, S.; McGale, P.; Correa, C.; Taylor, C.; Arriagada, R.; Clarke, M.; Cutter, D.; Davies, C.; Ewertz, M.; Godwin, J.; Gray, R.; Pierce, L.; Whelan, T.; Wang, Y.; Peto, R. Effect of Radiotherapy After Breast-Conserving Surgery on 10-Year Recurrence and 15-Year Breast Cancer Death: Meta-Analysis of Individual Patient Data for 10,801 Women in 17 Randomised Trials. *Lancet* **2011**, *378*, 1707−1716.

(3) Mellman, I.; Coukos, G.; Dranoff, G. Cancer Immunotherapy Comes of Age. *Nature* **2011**, *480*, 480−489.

(4) Chen, D. S.; Mellman, I. Oncology Meets Immunology: The Cancer-Immunity Cycle. *Immunity* **2013**, *39*, 1−10.

(5) Noy, R.; Pollard, J. W. Tumor-Associated Macrophages: from Mechanisms to Therapy. *Immunity* **2014**, *41*, 49−61.

(6) Ostuni, R.; Kratochvill, F.; Murray, P. J.; Natoli, G. Macrophages and Cancer: from Mechanisms to Therapeutic Implications. *Trends Immunol.* **2015**, *36*, 229−239.

(7) Biswas, S. K.; Mantovani, A. Macrophage Plasticity and Interaction with Lymphocyte Subsets: Cancer as a Paradigm. *Nat. Immunol.* **2010**, *11*, 889−896.

(8) Qian, B.-Z.; Pollard, J. W. Macrophage Diversity Enhances Tumor Progression and Metastasis. *Cell* **2010**, *141*, 39−51.

(9) Guerriero, J. L.; Sotayo, A.; Ponichtera, H. E.; Castrillon, J. A.; Pourzia, A. L.; Schad, S.; Johnson, S. F.; Carrasco, R. D.; Lazo, S.; Bronson, R. T.; Davis, S. P.; Lobera, M.; Nolan, M. A.; Letai, A. Class IIa HDAC Inhibition Reduces Breast Tumours and Metastases Through Anti-Tumour Macrophages. *Nature* **2017**, *543*, 428−432.

(10) Sica, A.; Mantovani, A. Macrophage Plasticity and Polarization: *in Vivo* Veritas. *J. Clin. Invest.* **2012**, *122*, 787−795.

(11) Okabe, Y.; Medzhitov, R. Tissue-Specific Signals Control Reversible Program of Localization and Functional Polarization of Macrophages. *Cell* **2014**, *157*, 832−844.

(12) Daldrup-Link, H. E.; Golovko, D.; Ruffell, B.; DeNardo, D. G.; Castaneda, R.; Ansari, C.; Rao, J.; Tikhomirov, G. A.; Wendland, M. F.; Corot, C.; Coussens, L. M. MRI of Tumor-Associated Macrophages with Clinically Applicable Iron Oxide Nanoparticles. *Clin. Cancer Res.* **2011**, *17*, 5695−5704.

(13) Huang, Z.; Zhang, Z.; Jiang, Y.; Zhang, D.; Chen, J.; Dong, L.; Zhang, J. Targeted Delivery of Oligonucleotides into Tumor-Associated Macrophages for Cancer Immunotherapy. *J. Controlled Release* **2012**, *158*, 286−292.

(14) Zhu, S.; Niu, M.; O'Mary, H.; Cui, Z. Targeting of Tumor-Associated Macrophages Made Possible by PEG-Sheddable, Mannose-Modified Nanoparticles. *Mol. Pharmaceutics* **2013**, *10*, 3525−3530.

(15) van Dam, G. M.; Themelis, G.; Crane, L. M. A.; Harlaar, N. J.; Pleijhuis, R. G.; Kelder, W.; Sarantopoulos, A.; de Jong, J. S.; Arts, H. J. G.; van der Zee, A. G. J.; Bart, J.; Low, P. S.; Ntziachristos, V. Intraoperative Tumor-Specific Fluorescence Imaging in Ovarian Cancer by Folate Receptor-A Targeting: First in-Human Results. *Nat. Med.* **2011**, *17*, 1315−1319.

(16) Napoletano, C.; Zizzari, I. G.; Rughetti, A.; Rahimi, H.; Irimura, T.; Clausen, H.; Wandall, H. H.; Belleudi, F.; Bellati, F.; Pierelli, L.; Frati, L.; Nuti, M. Targeting of Macrophage Galactose-Type C-Type Lectin (MGL) Induces DC Signaling and Activation. *Eur. J. Immunol.* **2012**, *42*, 936−945.

(17) Sallusto, F.; Cella, M.; Danieli, C.; Lanzavecchia, A. Dendritic Cells Use Macropinocytosis and the Mannose Receptor to Concentrate Macromolecules in the Major Histocompatibility Complex Class II Compartment: Downregulation by Cytokines and Bacterial Products. *J. Exp. Med.* **1995**, *182*, 389−400.

(18) Cieslewicz, M.; Tang, J.; Yu, J. L.; Cao, H.; Zavaljevski, M.; Motoyama, K.; Lieber, A.; Raines, E. W.; Pun, S. H. Targeted Delivery of Proapoptotic Peptides to Tumor-Associated Macrophages Improves Survival. *Proc. Natl. Acad. Sci. U. S. A.* **2013**, *110*, 15919−15924.

(19) Quail, D. F.; Bowman, R. L.; Akkari, L.; Quick, M. L.; Schuhmacher, A. J.; Huse, J. T.; Holland, E. C.; Sutton, J. C.; Joyce, J. A. The Tumor Microenvironment Underlies Acquired Resistance to CSF-1R Inhibition in Gliomas. *Science* **2016**, *352*, aad3018−aad3018.

(20) Lin, E. Y.; Nguyen, A. V.; Russell, R. G.; Pollard, J. W. Colony-Stimulating Factor 1 Promotes Progression of Mammary Tumors to Malignancy. *J. Exp. Med.* **2001**, *193*, 727−740.

(21) Pyonteck, S. M.; Akkari, L.; Schuhmacher, A. J.; Bowman, R. L.; Sevenich, L.; Quail, D. F.; Olson, O. C.; Quick, M. L.; Huse, J. T.; Teijeiro, V.; Setty, M.; Leslie, C. S.; Oei, Y.; Pedraza, A.; Zhang, J.; Brennan, C. W.; Sutton, J. C.; Holland, E. C.; Daniel, D.; Joyce, J. A. CSF-1R Inhibition Alters Macrophage Polarization and Blocks Glioma Progression. *Nat. Med.* **2013**, *19*, 1264−1272.

(22) Hume, D. A.; MacDonald, K. P. A. Therapeutic Applications of Macrophage Colony-Stimulating Factor-1 (CSF-1) and Antagonists of CSF-1 Receptor (CSF-1R) Signaling. *Blood* **2012**, *119*, 1810−1820.

(23) Cuellar, T. L.; Barnes, D.; Nelson, C.; Tanguay, J.; Yu, S.-F.; Wen, X.; Scales, S. J.; Gesch, J.; Davis, D.; van Brabant Smith, A.; Leake, D.; Vandlen, D.; Siebel, C. W. Systematic Evaluation of Antibody-Mediated siRNA Delivery Using an Industrial Platform of THIOMAB-siRNA Conjugates. *Nucleic Acids Res.* **2015**, *43*, 1189−1203.

(24) Zhao, N.; Pan, Y.; Cheng, Z.; Liu, H. Gold Nanoparticles for Cancer Theranostics-A Brief Update. *J. Innovative Opt. Health Sci.* **2016**, *09*, 1630004−1630010.

(25) Whitehead, K. A.; Langer, R.; Anderson, D. G. Knocking Down Barriers: Advances in siRNA Delivery. *Nat. Rev. Drug Discovery* **2010**, *9*, 412−412.

(26) Kanasty, R.; Dorkin, J. R.; Vegas, A.; Anderson, D. Delivery Materials for siRNA Therapeutics. *Nat. Mater.* **2013**, *12*, 967−977.

(27) Luo, H.; Lu, L.; Yang, F.; Wang, L.; Yang, X.; Luo, Q.; Zhang, Z. Nasopharyngeal Cancer-Specific Therapy Based on Fusion Peptide-Functionalized Lipid Nanoparticles. *ACS Nano* **2014**, *8*, 4334−4347.

(28) Huang, C.; Jin, H.; Qian, Y.; Qi, S.; Luo, H.; Luo, Q.; Zhang, Z. Hybrid Melittin Cytolytic Peptide-Driven Ultrasmall Lipid Nanoparticles Block Melanoma Growth *in Vivo*. *ACS Nano* **2013**, *7*, 5791−5800.

(29) Pluen, A.; Boucher, Y.; Ramanujan, S.; McKee, T. D.; Gohongi, T.; di Tomaso, E.; Brown, E. B.; Izumi, Y.; Campbell, R. B.; Berk, D. A.; Jain, R. K. Role of Tumor-Host Interactions in Interstitial Diffusion of Macromolecules: Cranial vs. Subcutaneous Tumors. *Proc. Natl. Acad. Sci. U. S. A.* **2001**, *98*, 4628−4633.



DOI: 10.1021/acsnano.7b05465
*ACS Nano* 2017, 11, 9536−9549

(30) De Palma, M.; Lewis, C. E. Macrophage Regulation of Tumor Responses to Anticancer Therapies. *Cancer Cell* **2013**, *23*, 277−286.
(31) Mantovani, A.; Sozzani, S.; Locati, M.; Allavena, P.; Sica, A. Macrophage Polarization: Tumor-Associated Macrophages as a Paradigm for Polarized M2Mononuclear Phagocytes. *Trends Immunol.* **2002**, *23*, 549−555.
(32) Dutta, P.; Hoyer, F. F.; Grigoryeva, L. S.; Sager, H. B.; Leuschner, F.; Courties, G.; Borodovsky, A.; Novobrantseva, T.; Ruda, V. M.; Fitzgerald, K.; Weissleder, R.; Nahrendorf, M. Macrophages Retain Hematopoietic Stem Cells in the Spleen *via* VCAM-1. *J. Exp. Med.* **2015**, *212*, 497−512.
(33) Lin, Q.; Chen, J.; Jin, H.; Ng, K. K.; Yang, M.; Cao, W.; Ding, L.; Zhang, Z.; Zheng, G. Efficient Systemic Delivery of siRNA by Using High-Density Lipoprotein-Mimicking Peptide Lipid Nanoparticles. *Nanomedicine* **2012**, *7*, 1813−1825.
(34) Qian, Y.; Jin, H.; Qiao, S.; Dai, Y.; Huang, C.; Lu, L.; Luo, Q.; Zhang, Z. Targeting Dendritic Cells in Lymph Node with an Antigen Peptide-Based Nanovaccine for Cancer Immunotherapy. *Biomaterials* **2016**, *98*, 171−183.
(35) DeNardo, D. G.; Barreto, J. B.; Andreu, P.; Vasquez, L.; Tawfik, D.; Kolhatkar, N.; Coussens, L. M. $CD4^+$ T Cells Regulate Pulmonary Metastasis of Mammary Carcinomas by Enhancing Protumor Properties of Macrophages. *Cancer Cell* **2009**, *16*, 91−102.
(36) Kumar, V.; Patel, S.; Tcyganov, E.; Gabrilovich, D. I. The Nature of Myeloid-Derived Suppressor Cells in the Tumor Microenvironment. *Trends Immunol.* **2016**, *37*, 208−220.
(37) Xu, J.; Escamilla, J.; Mok, S.; David, J.; Priceman, S.; West, B.; Bollag, G.; McBride, W.; Wu, L. CSF1R Signaling Blockade Stanches Tumor-Infiltrating Myeloid Cells and Improves the Efficacy of Radiotherapy in Prostate Cancer. *Cancer Res.* **2013**, *73*, 2782−2794.
(38) Hamilton, J. A. Colony-Stimulating Factors in Inflammation and Autoimmunity. *Nat. Rev. Immunol.* **2008**, *8*, 533−544.
(39) Zhu, Y.; Knolhoff, B. L.; Meyer, M. A.; Nywening, T. M.; West, B. L.; Luo, J.; Wang-Gillam, A.; Goedegebuure, S. P.; Linehan, D. C.; DeNardo, D. G. CSF1/CSF1R Blockade Reprograms Tumor-Infiltrating Macrophages and Improves Response to T-Cell Checkpoint Immunotherapy in Pancreatic Cancer Models. *Cancer Res.* **2014**, *74*, 5057−5069.
(40) Ruffell, B.; Chang-Strachan, D.; Chan, V.; Rosenbusch, A.; Ho, C. M. T.; Pryer, N.; Daniel, D.; Hwang, E. S.; Rugo, H. S.; Coussens, L. M. Macrophage IL-10 Blocks $CD8^+$ T Cell-Dependent Responses to Chemotherapy by Suppressing IL-12 Expression in Intratumoral Dendritic Cells. *Cancer Cell* **2014**, *26*, 623−637.
(41) Wherry, E. J. T Cell Exhaustion. *Nat. Immunol.* **2011**, *12*, 492−499.
(42) Ries, C. H.; Cannarile, M. A.; Hoves, S.; Benz, J.; Wartha, K.; Runza, V.; Rey-Giraud, F.; Pradel, L. P.; Feuerhake, F.; Klaman, I.; Jones, T.; Jucknischke, U.; Scheiblich, S.; Kaluza, K.; Gorr, I. H.; Walz, A.; Abiraj, K.; Cassier, P. A.; Sica, A.; Gomez-Roca, C.; et al. Targeting Tumor-Associated Macrophages with Anti-CSF-1R Antibody Reveals a Strategy for Cancer Therapy. *Cancer Cell* **2014**, *25*, 846−859.
(43) Luo, Y.; Zhou, H.; Krueger, J.; Kaplan, C.; Lee, S.-H.; Dolman, C.; Markowitz, D.; Wu, W.; Liu, C.; Reisfeld, R. A.; Xiang, R. Targeting Tumor-Associated Macrophages as a Novel Strategy Against Breast Cancer. *J. Clin. Invest.* **2006**, *116*, 2132−2141.
(44) Conde, J.; Bao, C.; Tan, Y.; Cui, D.; Edelman, E. R.; Azevedo, H. S.; Byrne, H. J.; Artzi, N.; Tian, F. Dual Targeted Immunotherapy *via in Vivo* Delivery of Biohybrid RNAi-Peptide Nanoparticles to Tumor-Associated Macrophages and Cancer Cells. *Adv. Funct. Mater.* **2015**, *25*, 4183−4194.
(45) Murray, P. J.; Wynn, T. A. Protective and Pathogenic Functions of Macrophage Subsets. *Nat. Rev. Immunol.* **2011**, *11*, 723−737.
(46) Robinson, M. W.; Harmon, C.; O'Farrelly, C. Liver Immunology and Its Role in Inflammation and Homeostasis. *Cell. Mol. Immunol.* **2016**, *13*, 267−276.
(47) Out, R.; Hoekstra, M.; Spijkers, J. A. A.; Kruijt, J. K.; van Eck, M.; Bos, I. S. T.; Twisk, J.; Van Berkel, T. J. C. Scavenger Receptor Class B Type I Is Solely Responsible for the Selective Uptake of Cholesteryl Esters from HDL by the Liver and the Adrenals in Mice. *J. Lipid Res.* **2004**, *45*, 2088−2095.
(48) Ikarashi, M.; Nakashima, H.; Kinoshita, M.; Sato, A.; Nakashima, M.; Miyazaki, H.; Nishiyama, K.; Yamamoto, J.; Seki, S. Distinct Development and Functions of Resident and Recruited Liver Kupffer Cells/Macrophages. *J. Leukocyte Biol.* **2013**, *94*, 1325−1336.
(49) Wang, C.; Yu, X.; Cao, Q.; Wang, Y.; Zheng, G.; Tan, T. K.; Zhao, H.; Zhao, Y.; Wang, Y.; Harris, D. C. Characterization of Murine Macrophages from Bone Marrow, Spleen and Peritoneum. *BMC Immunol.* **2013**, *14*, 6−15.
(50) Zasłona, Z.; Wilhelm, J.; Cakarova, L.; Marsh, L. M.; Seeger, W.; Lohmeyer, J.; von Wulffen, W. Transcriptome Profiling of Primary Murine Monocytes, Lung Macrophages and Lung Dendritic Cells Reveals a Distinct Expression of Genes Involved in Cell Trafficking. *Respir. Res.* **2009**, *10*, 2−18.
(51) Chen, Y.; Xia, R.; Huang, Y.; Zhao, W.; Li, J.; Zhang, X.; Wang, P.; Venkataramanan, R.; Fan, J.; Xie, W.; Ma, X.; Lu, B.; Li, S. An Immunostimulatory Dual-Functional Nanocarrier That Improves Cancer Immunochemotherapy. *Nat. Commun.* **2016**, *7*, 13443−13455.
(52) Qi, S.; Li, H.; Lu, L.; Qi, Z.; Liu, L.; Chen, L.; Shen, G.; Fu, L.; Luo, Q.; Zhang, Z. Long-Term Intravital Imaging of the Multicolor-Coded Tumor Microenvironment During Combination Immunotherapy. *eLife* **2016**, *5*, 3160−3188.
(53) Tabas, I. Macrophage Death and Defective Inflammation Resolution in Atherosclerosis. *Nat. Rev. Immunol.* **2010**, *10*, 36−46.
(54) Prima, V.; Kaliberova, L. N.; Kaliberov, S.; Curiel, D. T.; Kusmartsev, S. COX2/mPGES1/PGE2 Pathway Regulates PD-L1 Expression in Tumor-Associated Macrophages and Myeloid-Derived Suppressor Cells. *Proc. Natl. Acad. Sci. U. S. A.* **2017**, *114*, 1117−1122.
(55) Noman, M. Z.; Desantis, G.; Janji, B.; Hasmim, M.; Karray, S.; Dessen, P.; Bronte, V.; Chouaib, S. PD-L1 Is a Novel Direct Target of HIF-1$\alpha$, and Its Blockade Under Hypoxia Enhanced MDSC-Mediated T Cell Activation. *J. Exp. Med.* **2014**, *211*, 781−790.
(56) Zhang, Z.; Chen, J.; Ding, L.; Jin, H.; Lovell, J. F.; Corbin, I. R.; Cao, W.; Lo, P.-C.; Yang, M.; Tsao, M.-S.; Luo, Q.; Zheng, G. HDL-Mimicking Peptide-Lipid Nanoparticles with Improved Tumor Targeting. *Small* **2010**, *6*, 430−437.
(57) Gabrilovich, D. I.; Ostrand-Rosenberg, S.; Bronte, V. Coordinated Regulation of Myeloid Cells by Tumours. *Nat. Rev. Immunol.* **2012**, *12*, 253−268.
(58) Cho, N.-H.; Cheong, T.-C.; Min, J. H.; Wu, J. H.; Lee, S. J.; Kim, D.; Yang, J.-S.; Kim, S.; Kim, Y. K.; Seong, S.-Y. A Multifunctional Core-Shell Nanoparticle for Dendritic Cell-Based Cancer Immunotherapy. *Nat. Nanotechnol.* **2011**, *6*, 675−682.
(59) Movita, D.; Kreefft, K.; Biesta, P.; van Oudenaren, A.; Leenen, P. J. M.; Janssen, H. L. A.; Boonstra, A. Kupffer Cells Express a Unique Combination of Phenotypic and Functional Characteristics Compared with Splenic and Peritoneal Macrophages. *J. Leukocyte Biol.* **2012**, *92*, 723−733.


DOI: 10.1021/acsnano.7b05465
*ACS Nano* 2017, 11, 9536−9549